

**TURBULENT COLLISION STATISTICS OF CLOUD DROPLETS
AT LOW DISSIPATION RATES**

by

Sandipan Banerjee

A thesis submitted to the Faculty of the University of Delaware in partial fulfillment of the requirements for the degree of Master of Science in Mechanical Engineering

Summer 2016

© 2016 Sandipan Banerjee
All Rights Reserved

ProQuest Number: 10190992

All rights reserved

INFORMATION TO ALL USERS

The quality of this reproduction is dependent upon the quality of the copy submitted.

In the unlikely event that the author did not send a complete manuscript and there are missing pages, these will be noted. Also, if material had to be removed, a note will indicate the deletion.



ProQuest 10190992

Published by ProQuest LLC (2016). Copyright of the Dissertation is held by the Author.

All rights reserved.

This work is protected against unauthorized copying under Title 17, United States Code
Microform Edition © ProQuest LLC.

ProQuest LLC.
789 East Eisenhower Parkway
P.O. Box 1346
Ann Arbor, MI 48106 - 1346

**TURBULENT COLLISION STATISTICS OF CLOUD DROPLETS
AT LOW DISSIPATION RATES**

by

Sandipan Banerjee

Approved: _____
Lian-Ping Wang, Ph.D.
Professor in charge of thesis on behalf of the Advisory Committee

Approved: _____
Suresh G. Advani, Ph.D.
Chair of the Department of Mechanical Engineering

Approved: _____
Babatunde A. Ogunnaike, Ph.D.
Dean of the College of Engineering

Approved: _____
Ann L. Ardis, Ph.D.
Senior Vice Provost for Graduate and Professional Education

ACKNOWLEDGMENTS

I would first like to thank my advisor, Prof. Lian-Ping Wang, for providing me the opportunity to work and learn under him. I thank him for exposing me to high quality research standards, for sharing his valuable expertise, and for guiding me through the course of my graduate studies at University of Delaware.

I thank Dr. Ajay Prasad, Dr. Leonard Schwartz, and Dr. Orlando Ayala for being on my thesis committee. Special thanks to Dr. Ayala for his constant guidance throughout my time here at Delaware through skype sessions. Our conversations, be it technical or motivational, always inspired me to work harder. I learnt a lot from him.

From oceans apart I thank my parents for their support and blessings. I would also like to thank my lab mates: Mr. Cheng Peng, Mr. Harish Opadrishta, Mr. Haoda Min, Ms. Xin Wen, Ms. Queming Qiu, and Dr. Hossein Parishani for all the great times we had in and out of the lab.

I thank my wife, Preetha, for her constant support and understanding, especially when the times were hard. Thank you for your patience, and keeping me patient. This thesis is dedicated to you.

Finally, I would like to acknowledge the financial support by National Science Foundation (NSF) and National Center for Atmospheric Research (NCAR). All the simulations were conducted on the Yellowstone supercomputer at NCAR.

TABLE OF CONTENTS

LIST OF TABLES	vi
LIST OF FIGURES	viii
ABSTRACT	x
 Chapter	
1 INTRODUCTION	1
1.1 Background & Motivation	1
1.2 Direct Numerical Simulation (DNS) Relevant To Cloud Physics	4
1.3 Specific Objectives	7
2 COLLISION STATISTICS IN STILL FLUID AND TURBULENT FLOWS	9
2.1 Collision Statistics In Still Fluid	9
2.1.1 Collision detection	11
2.1.2 Prediction of relative percentages of collision of different Types	13
2.1.3 Pair and collision statistics	15
2.1.4 Uncertainty analysis for collision kernel: gravity only case	17
2.1.5 Results for collision kernel: gravity only case	21
2.1.6 Collision statistics for gravity only with hydrodynamic interactions	22
2.2 Collision Statistics In Turbulent Flow	26
2.2.1 Uncertainty for collision kernel in turbulent flow case	27
2.2.2 Collision kernel results in a turbulent flow	30
2.2.3 Collision efficiency and collision efficiency enhancement	33

3 ASYMPTOTIC EXPANSION APPROACH FOR PARTICLE TRACKING	36
3.1 Motivation & Background	36
3.2 The Asymptotic Expansion	38
3.3 Validation Of The Asymptotic Expansion For 2-D Cellular Flow . . .	43
3.4 Asymptotic Expansion In Turbulent Flow	45
3.4.1 Run time comparison	51
4 SUMMARY AND CONCLUSION	53
REFERENCES	55

LIST OF TABLES

1.1	Particle Stokes number and non-dimensional settling velocities at different dissipation rates	7
2.1	Collision kernel with standard deviation for 30-40 μm radius particles for gravity only and NoHI case	21
2.2	Collision kernel with standard deviation for 30-40 μm radius particles for gravity only and with HI case	25
2.3	Collision efficiency with standard deviation for 30-40 μm radius particles for gravity only	26
2.4	Collision kernel with standard deviation comparison for dissipation rate 100 cm^2/sec^3	29
2.5	Collision kernel with standard deviation for 30-40 μm radius particles for dissipation rate 3 cm^2/sec^3	31
2.6	Collision kernel with standard deviation for 30-40 μm radius particles for dissipation rate 10 cm^2/sec^3	32
2.7	Collision kernel with standard deviation for 30-40 μm radius particles for dissipation rate 30 cm^2/sec^3	32
2.8	Collision kernel with standard deviation for 30-40 μm radius particles for dissipation rate 100 cm^2/sec^3	33
2.9	Collision efficiency with standard deviation for 30-40 μm radius particles in turbulent flow	34
3.1	Comparison of w_r for existing approach and asymptotic approach	49
3.2	Comparison of RDF, ($g(r)$) for existing approach and asymptotic approach	50

3.3	Comparison of collision kernel, (Γ) for existing approach and asymptotic approach	51
3.4	Comparison of run time for existing approach and asymptotic approach	52

LIST OF FIGURES

2.1	The DNS computational Domain	10
2.2	Repetition after $L_b/\Delta W$. This sketch is made by taking a frame of reference fixed on the smaller particles and observe the relative motion of larger particles.	11
2.3	Grid for collision detection	12
2.4	Prediction of collision type 1 and 2: geometry	14
2.5	Comparison of theory and simulation for type 2 collisions	16
2.6	Spherical shell and RDF	16
2.7	Auto-Correlation for gravity only	20
2.8	Initial position bias	22
2.9	Auto-Correlation for dissipation rate of $10cm^2/sec^3$; Here $m = (5 * dt)$, so $m/Deltat = (0.00152/(L_b/\Delta W))$	28
2.10	Comparison of collision efficiency enhancement with linear interpolation	35
3.1	Particle trajectory comparison for asymptotic and existing approach in 2D cellular flow	44
3.2	Relative error of position between the two methods as a function of time	45
3.3	Particle trajectory comparison for asymptotic and existing approach in turbulent flow (x vs y)	46
3.4	Particle trajectory comparison for asymptotic and existing approach in turbulent flow (x vs z)	47

3.5	Relative error of r position (calculated by $r = \sqrt{x^2 + y^2}$) as a function of time for asymptotic method compared to the direct integration method	48
3.6	Relative error of r position (calculated by $r = \sqrt{x^2 + z^2}$) as a function of time for asymptotic method compared to the direct integration method	49

ABSTRACT

Collisions of sedimenting droplets in a turbulent flow is of great importance in cloud physics. Collision efficiency and collision enhancement over gravitational collision by air turbulence govern the growth of the cloud droplets leading to warm rain initiation and precipitation dynamics. In this thesis we present direct numerical simulation (DNS) results for collision statistics of droplets in turbulent flows of low dissipation rates (in the range of $3 \text{ cm}^2/\text{s}^3$ - $100 \text{ cm}^2/\text{s}^3$) relevant to strato-cumulus clouds.

First, we revisit the case of gravitational collision in still fluid to validate the details of the collision detection algorithm used in our code. We compare the collision statistics with either new analytical predictions regarding the percentages of different collision types, or results from published papers. The effect of initial conditions on the collision statistics and statistical uncertainties are analyzed both analytically and through the simulation data.

Second, we consider the case of weak turbulence (as in strato-cumulus clouds). In this case the particle motion is mainly driven by gravity. The standard deviation (or the uncertainty) of the average collision statistics is examined analytically in terms of time correlation function of the data. We then report new DNS results of collision statistics in a turbulent flow, showing how air turbulence increases the geometric collision statistics and the collision efficiency. We find that the collision-rate enhancement due to turbulence depends nonlinearly on the flow dissipation rate. This result calls for a more careful parameterization of the collision statistics in strato-cumulus clouds.

Due to the low flow dissipation rate in stratocumulus clouds, a related challenge is low droplet Stokes number. Here the Stokes number is the ratio of droplet inertial response time to the flow Kolmogorov time. A very low Stokes number implies that the numerical integration time step is now governed by the droplet inertial response

time, rather than the time step necessary for the flow simulation. This situation makes the simulations very expensive to perform. With the motivation to speed up the simulations, we implement the asymptotic expansion approach (as in Maxey, 1987) for particle tracking as this method is suitable for low particle Stokes number and avoids the numerical integration of the stiff equation of motion of droplets. We first validate our implementation using the simpler 2-D cellular flow. Next, we compare the collision statistics of the newly implemented asymptotic approach with our existing approach of particle tracking as well as with published results from journal papers. Finally, we provide the run time comparison for both methods.

Chapter 1

INTRODUCTION

1.1 Background & Motivation

Particle laden turbulent flows are commonly found in both natural as well as industrial flows; raindrop growth in the clouds, aerosol processing, and pneumatic transport of solids are some examples. In these flows, the particle-particle collision and coagulation processes affect the dynamics (such as flow drag) and evolution (e.g., the growth of particles) of the system. The rate of coagulation is determined by the geometric collision rate, the collision efficiency, and the coagulation efficiency. The geometric collision is affected by the carrier turbulent flow due to the effects of turbulence on the relative motion and the local distributions of the inertial particles (Sundaram & Collins, 1997, Wang et al. 1998a, 2000). The collision efficiency is affected by the local particle-particle hydrodynamic interactions due to disturbance flows induced by the particles (Wang et al. 1998a, 2000). The coagulation efficiency is governed by interfacial forces such as the surface tension and van der Waals force, etc. This thesis focuses on raindrop growth in clouds by collision-coalescence, specifically for stratocumulus clouds where the viscous dissipation rate is relatively low. Our main concern is the geometric collision rates and collision efficiency of cloud droplets.

Rain develops when liquid droplets collide with each other to form a particle of larger size, this process is called collision-coalescence. The coalescence process goes on until the droplets reach the size of a rain-drop, and become too heavy to be suspended in the air, resulting in rainfall. It is quite understandable that more collisions between cloud droplets would result in higher rate of coalescence, and the rate of collision would depend on the relative velocity between particles. If a particle has a larger

settling velocity, the probability of that particle to collide with a smaller particle would be higher, and thus coalescence would be faster due to differential sedimentation (or gravitational collision-coalescence). It is evident that particles with larger size, and hence larger inertia would have higher settling velocity. It is well known that this gravitational coagulation is a dominant growth mechanism for larger particles (larger than $40 \mu m$ radius) (Pruppacher and Klett, 1997, Grabowski and Wang, 2013). In the case of particles smaller than that, the still fluid settling velocity is smaller. This combined with low collision-efficiency (Wang et al. 2005, Wang et al. 2008) makes the rate of particle-particle collision to be relatively slow.

In the early stage of cloud droplet formation and growth (say below $15 \mu m$ in radius), water vapor condensation (driven by local super-saturation) is the dominant mechanism for droplet growth. However, the rate of growth due to condensation is inversely proportional to the particle size as the vapor concentration gradient at the droplet surface reduces with increase in radius. For example, it would take about 1 hr for a $15 \mu m$ droplet to grow up to $50 \mu m$ radius, by the diffusion mechanism alone (Pruppacher and Keltt, 1997). Furthermore, the water vapor in the air is limited, as such the local super-saturation decreases as more water is converted from vapor to liquid.

On the contrary, the conclusions based on observations in real clouds is very different. It was first observed by Squires (1958), that the rain formation period could be less than half an hour. More recently, with the use of radar technology, it was observed that warm rain initiation in cumulus clouds could be as short as 15-20 minutes (Szumowski et al., 1997, Knight et al., 2002). It should be noted that there were some debates about the difficulties in interpreting data from radar measurements (Rauber et al., 2003; Knight et al., 2002), specifically distinguishing between cloud region and clear region from radar images and satellite images. In 2007, Rauber et al. published results which were gathered from air-crafts with measurement equipments, flying directly in cumulus clouds, putting the radar and satellite images debate to rest. The results conclude that the rain formation time in shallow cumulus clouds over the ocean is

about 20-30 minutes. This led to a gap in the physical explanation and experimental results.

The two mechanisms of growth of droplets: condensation and coalescence, both are not very effective in the size range of $15 \mu m$ to $40 \mu m$ in radius, and definitely not effective enough to make the rain formation time to be in the range 20-30 minutes. This problem is called as the “size-gap problem” in cloud physics. The example of 1 hr taken by $15 \mu m$ particles to grow to $50 \mu m$ (Pruppacher and Klett, 1997) is a good example for this. So there must be some mechanism which either enhances the collision rate and hence the coalescence process or which enhances the condensation process.

Although there has been a lot of work done on the effects of turbulence on the condensation process, in this thesis we focus mainly on the work with the coalescence process (specifically enhancement of collision rate, and other collision related parameters which would be discussed later in the thesis). The studies conducted in relation to the coalescence process mainly point towards the effect of air turbulence. Specifically, the coagulation rate of finite sized particles in fluid turbulence, which is governed by three consecutive processes (Wang et al., 2000):

(1) Geometric Collision due to particle-turbulence interactions: This is the physical collision between two particles, where the motion of the particles is driven by the turbulent flow and gravitational sedimentation.

(2) Collision efficiency due to particle-particle aerodynamic interaction: It is the effect of the presence of one particle on the motion of the neighboring particles. Presence of a particle distorts the flow. When two particles are close to each other, the distortion in the flow created by one particle is “felt” by the other particle, and vice-versa. Thus, the first particle is pushing the fluid, and the fluid is pushing the second particle (and vice-versa). Due to this motion, the particles may avoid collision by moving away from each other because of the pressure difference. This effect is called the particle-particle aerodynamic interaction, which would prevent particle-particle collision and thus reduce the total number of collisions as the particles move

away from each other. Collision efficiency is the ratio of the collision rate considering this aerodynamic interaction effect to the collision rate without considering this aerodynamic interaction effect.

(3) Coagulation efficiency (when two particles join to form a third one): This is a result of mainly two competing effects for water droplets: one is the van der Waals attractive force (which pulls two particles together) and the other is the surface tension (which maintains the interfaces and lubrication forces that tend to pull particles apart).

1.2 Direct Numerical Simulation (DNS) Relevant To Cloud Physics

Since the air motion in clouds is of turbulent nature, there have been many studies on the effect of turbulence in the enhancement of collision-coalescence which relates the intensity of air turbulence and particle inertia to the increase of collision-coalescence. Some of these studies were in qualitative agreement (Almeida, 1976, 1979, Pinsky et al, 1999, 2000, Prupachher and Klett, 1997) and some were in disagreement on the theory of turbulence enhancing the collision rate (Koziol and Leighton, 1996). On the quantitative level, there had been no general consensus until relatively recently. The recent advance is largely due to rigorous simulation studies by Sundaram and Collins, 1997, Khain and Pinsky, 1997, Wang et al 2000, who provide evidence of turbulence enhancing the collision rate. The above studies helped in providing a better understanding of the effects of turbulence on collisions. However, as these studies were based on engineering applications, the flow dissipation rates were very large and particle sedimentation was often not considered. In clouds, the dissipation rates are much smaller.

Numerical simulation results from Wang et al. (2008) and Ayala et al. (2008) have helped in quantifying the effects of turbulence on the collision rate, for clouds through a rigorous direct numerical simulation of dispersed turbulent flow which was based on the classical work of Wang and Maxey 1993 and Wang et al. 2000. A lot of progress has already been made by our group led by Prof. Lian-Ping Wang (Wang et al.

2000, 2005a, 2005b, 2006, 2007, 2008, 2009, Ayala et al., 2008, Wang and Grabowski, 2009, and many more). My research work is to extend the work by determining the collision statistics at low flow dissipation rates (relevant to strato-cumulus clouds).

In this work we study collision of cloud droplets by direct numerical simulations where the background turbulent flow is generated by solving the incompressible Navier-Stokes equation using a pseudo-spectral method. The particles are then added and tracked by using the equation of motion. Multiple processors are used to perform the simulations, hence the domain is divided in two directions (y and z in our code), also called 2-D domain decomposition so that each processor contains a “pencil” portion of the domain. Data communication between processors are done using MPI. Further details about the equations involved and the implementation technique will be provided in the subsequent chapters of this thesis. The presence of the particles are assumed to not have any effect of the background turbulence as the volume fraction is of the order of 10^{-6} . The smallest scales of the turbulence are defined by the Kolmogorov scales, namely:

Kolmogorov length scale:

$$\eta = (\nu^3/\epsilon)^{1/4} \quad (1.1)$$

Kolmogorov velocity scale:

$$v_k = (\nu\epsilon)^{1/4} \quad (1.2)$$

Kolmogorov time scale:

$$\tau_k = (\nu/\epsilon)^{1/2} \quad (1.3)$$

where ϵ is the average viscous dissipation rate of the turbulence and ν is the air kinematic viscosity.

The air viscosity is taken to be $\nu = 0.17\text{cm}^2/\text{s}$, and air density, $\rho = 0.001\text{gm}/\text{cm}^3$. Another important parameter that characterizes the turbulence in cloud is the Taylor microscale Reynolds number (R_λ). It is defined as:

$$R_\lambda = u'\lambda/\nu \quad (1.4)$$

where λ is the transverse Taylor microscale, defined as:

$$\lambda = u' / \langle (\partial u_1 / \partial x_1)^2 \rangle^{1/2} = (15\nu u'^2 / \epsilon)^{1/2} \quad (1.5)$$

and u' is the r.m.s. fluctuation velocity in a given direction.

As for the particles, we typically use particle sizes in the range of 5-40 μm in radius. The droplets are governed by the particle equation of motion, under the application of Stokes drag:

$$\frac{dV(t)}{dt} = \frac{U(Y(t)) - V(t)}{\tau_p} + g \quad (1.6)$$

where $V(t)$ is the velocity of the particle, $U(Y(t))$ is the fluid velocity at the particle location. It is calculated in the code by a six-point Lagrangian interpolation technique, g is the acceleration due to gravity, τ_p is the particle inertial response time (the time taken by the particle to react to a change in the flow) and, under Stokes drag it is given by:

$$\tau_p = 2\rho_w a^2 / 9\rho\nu \quad (1.7)$$

where $\rho_w = 1gm/cm^3$ is the density of the particles (water), and a is the particle radius.

The still fluid settling velocity of the particle is determined by the equation:

$$v_p = \tau_p |g| \quad (1.8)$$

There are two important non-dimensional parameters in this problem, and this would be a good place to define them. The first is the Stokes number, it is defined as the ratio of the particle inertial response time to the smallest time scale of the turbulence (Kolmogorov time-scale):

$$St = \tau_p / \tau_k \quad (1.9)$$

The other one is the non-dimensional settling velocity, which is defined as the ratio of the particle velocity to the Kolmogorov velocity scale:

$$Sv = v_p / v_k \quad (1.10)$$

Table 1.1 provides a list of particle radius with the respective Stokes number (St) and non-dimensional settling velocity (Sv) at particular dissipation rates. We note that the Stokes number decreases as particle size and flow dissipation rate are reduced.

Table 1.1: Particle Stokes number and non-dimensional settling velocities at different dissipation rates

Particle radius(μm)	Dissipation rates (cm^2/s^3)							
	3		10		30		100	
	St	Sv	St	Sv	St	Sv	St	Sv
5	0.0013	0.378	0.002	0.280	0.0043	0.2131	0.0079	0.1577
10	0.0054	1.515	0.010	1.121	0.0173	0.8524	0.0317	0.6308
20	0.0219	6.063	0.040	4.487	0.0694	3.4098	0.1268	2.5235
30	0.0494	13.64	0.090	10.097	0.1562	7.6721	0.2853	5.6779
40	0.0878	24.25	0.160	17.95	0.2778	13.639	0.5072	10.094

1.3 Specific Objectives

The main objective of this thesis is performing simulations relevant to cloud droplets in strato-cumulus clouds where dissipation rates are very low (below $100 cm^2/s^3$), and the particle St is relatively small. It should be noted that in case of a combination of small dissipation rate and small particle size, the time-step size required to numerically integrate equation 1.6 would be very small, and thus the simulations would become computationally very expensive (details provided in Chapter 3). The asymptotic expansion tracking of Maxey (1987) for particles with low Stokes number would be valid in this range. With the asymptotic expansion approach we can use larger time step sizes, and thus the code would become faster. In order to validate our

implementation of the asymptotic expansion, we use it first on a simple 2-D cellular flow (as in Maxey, 1987) and then in a turbulent flow.

The remainder of this thesis is divided into three chapters, the Chapter 2 consists of a reconsideration of the collision statistics in still fluid, which also consists of a description and theoretical prediction of the collision detection algorithm implemented in the code, finally it deals with the collision statistics in turbulent flow at low dissipation rates. Chapter 3 deals with the theory, implementation, results, and analysis of the asymptotic expansion method of particle tracking for the 2D cellular flow (as a validation) and then for turbulent flows. Finally, Chapter 4 summarizes the work done, its implications, and future research directions.

Chapter 2

COLLISION STATISTICS IN STILL FLUID AND TURBULENT FLOWS

Collisions between two particles occur due to the movement of the particles. There are three main aspects which govern the motion of a particle: effect of particle settling velocity, effect of transport by the fluid velocity through the hydrodynamic drag on the particle, and effect of particle-particle hydrodynamic interactions. In order to quantify the effect of each of these aspects, we need to study them one by one.

2.1 Collision Statistics In Still Fluid

In this section we revisit the so-called ‘gravity only case’. The main motivation to revisit the gravity only case is to figure out an accurate expression for the standard deviation of the collision kernel, in order to better understand the collision statistics in a turbulent flow. Under the influence of weak turbulence, the particle motion would be mainly driven by the gravity, hence a revisitation of the gravity case is required as a base reference case. In the gravity only case, the fluid is stationary, and the particle-particle hydrodynamic interactions (denoted as HI from here on) are ignored, so the particle motion is only due to gravity, which is quantified by the Stokes terminal velocity of the particle. We also perform some simulations by considering the HI effect for the gravity only case, in order to determine the collision efficiency in this case. We re-scale the cloud problem in DNS in a periodic box of length of $L_b = 2\pi = 6.283$ (in DNS units) (figure 2.1 shows the domain), and match the liquid water content (LWC) with the cloud. LWC is the mass of liquid per unit volume, basically this quantity determines the number of particles present in the system, a lower value of LWC means less number of particles, and higher value signifies larger number of particles. Typically

in strato-cumulus clouds, the LWC is about $1\text{gm}/\text{m}^3$, however, for our simulations (in some cases), we use a LWC value of $4\text{gm}/\text{m}^3$, as with more particles, more collisions can be realized, leading to lower standard deviation as the sample size becomes larger.

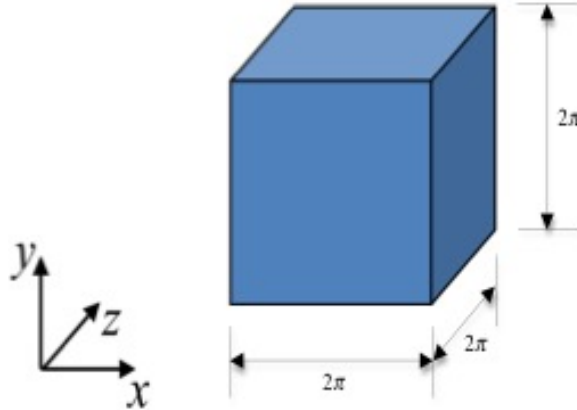


Figure 2.1: The DNS computational Domain

Typically we use a bidisperse system with particles of two different sizes. For our simulation results, we use two particle radii of $30\mu\text{m}$ and $40\mu\text{m}$. The particle initial positions are set using a uniform random distribution, and the particle initial velocity is set to the respective settling velocity. For the particle sedimentation driven by gravity only case, the particles settle with their sedimentation velocity in still fluid. The particle velocity is non-zero only in the gravity direction, as there is no horizontal motion. This means that the particles will collide because of the relative motion between them. Now, the relative motion between same size particles will be zero, as they have same the settling velocity. This means there will be no collision between same-size particles. For cross-size collisions, we can see that the entire scenario would repeat itself after every $L_b/\Delta W$ time due to the periodic boundary conditions, where $\Delta W = W_1 - W_2$, where W_1 , and W_2 are the settling velocities for the two sets of particles. Figure 2.2 shows a schematic of the domain with particles, after a time of

$L_b/\Delta W$. This means that the collision statistics will depend on the initial particle position only. So, with a random initial position distribution of the particles, the collision results would be biased. In order to get rid of the bias, we need to run multiple realizations of the simulation with different random initial distributions and average the data over all of them.

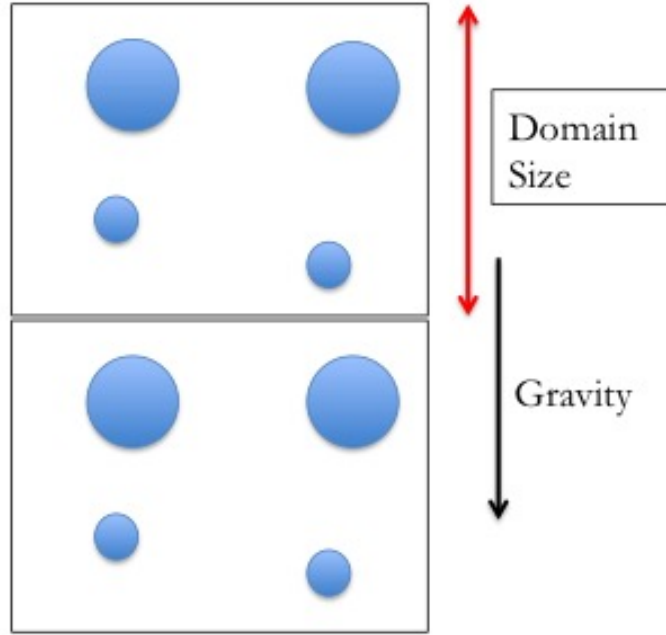


Figure 2.2: Repetition after $L_b/\Delta W$. This sketch is made by taking a frame of reference fixed on the smaller particles and observe the relative motion of larger particles.

2.1.1 Collision detection

The collision detection algorithm follows Wang et al. 1998a. A collision is defined as an event when the distance between the centers of two particles d_c is less than or equal to the sum of their radii or the geometric collision radius, R . In order to not miss any of the collisions, Wang et al. defined three types of collision.

Collision Type 1: When d_c is greater than R at the beginning of a time-step, and d_c is less than or equal to R , at the end of the time-step, then it is collision type 1.

Collision Type 2: When d_c is greater than R at the beginning of a time-step, and d_c remains greater than R at the end of the time-step, then a collision event may take place if in between the time-step, d_c became less than R . If d_c , indeed becomes less than R , at some time between the time-step, then a collision event must be recorded as collision type 2.

Collision Type 3: When d_c is less than or equal to R at the beginning of a time-step, and d_c remains less than or equal to R at the end of the time-step, then a collision event may take place in between the time step, if d_c becomes larger than R in that span of time. This is collision type 3.

The sum of these three types of collision would give the total number of collisions.

Next, we take a look at the collision detection algorithm. A primary detection grid (blue lines) of cell size W was introduced. Along with this, a second grid (red lines) of the same cell size but shifted in each direction by $W/2$ was also included.

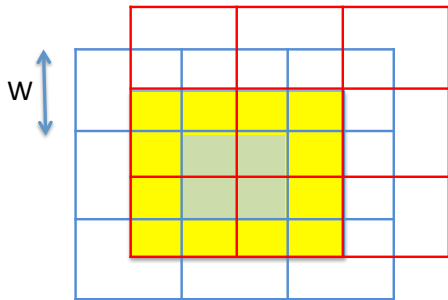


Figure 2.3: Grid for collision detection

Each particle's location was identified first with a cell in the primary grid. Let us suppose that the green cell at the center be the one where the particle was detected. The collision detection for this particle was restricted to a neighborhood defined as the region formed by the eight cells (shown as 4 cells as this image is in 2-D in yellow color) in the second grid that overlapped with the cell in primary grid, where the particle was found. To count the collisions, the algorithm selects a particle, identifies the primary cell, checks for other particles in the same primary cell and

in the neighborhood mentioned above in all directions. Thus the minimum distance between two particles that are not considered for collision is $W/2$. So, in case of a turbulent flow, we set the width of the detection grid to be $W > 2((R/dx)+10u'/dt)*dx$. where $10u'/dt$ is an upper bound for the relative velocity, and u' is the rms fluid fluctuating velocity. In case of sedimentation due to gravity only, we scale it with ΔW .

2.1.2 Prediction of relative percentages of collision of different Types

Since we are considering a relatively simple case of particle sedimentation under the influence of gravity in still fluid, the collision types can be predicted. First we note that collisions can occur only between different size particles, as same size particles will have no relative motion. Next, we notice that type 3 collision mentioned above would not occur in this problem as a particle pair cannot overlap each other twice. It turns out with the help of some geometry we can predict the Type 1 and Type 2 collisions.

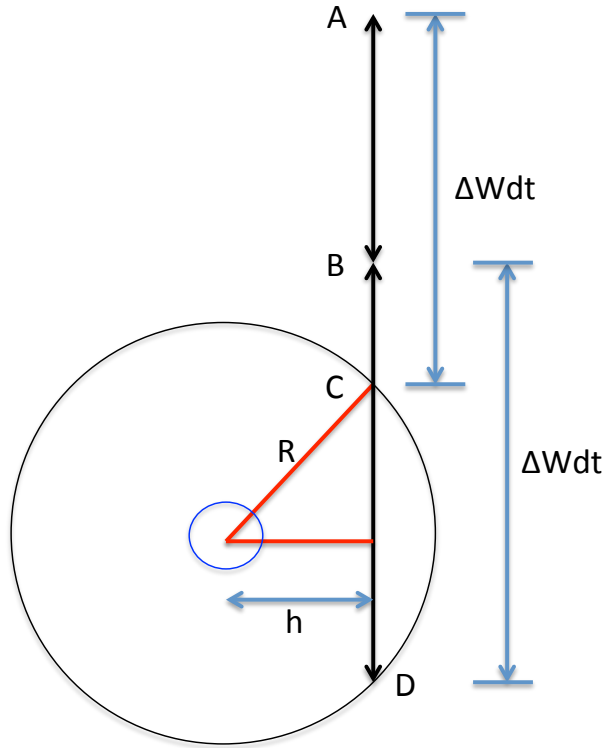


Figure 2.4: Prediction of collision type 1 and 2: geometry

In figure 2.4, we take a frame of reference fixed on the smaller particle and observe the trajectory of the larger particle, we assume the center of the larger particle is located on the line ABC. If the horizontal separation between two particles is h , then Type 2 collision will occur only when the length CD is less than $\Delta W dt$, which implies that

$$h > \sqrt{R^2 - \left(\frac{\Delta W dt}{2}\right)^2} = h_1 \quad (2.1)$$

where dt is the time step size used for the simulation. Clearly, only when the center of larger particle is located between A and C at the begin of the time step will collide with the smaller particle within the time step. Fraction of Type 1 collisions will be

AB/AC , and fraction of Type 2 collisions will be BC/AC . If we focus on Type 2 collision prediction, we can see that,

$$BC/AC = \frac{\Delta W dt - 2\sqrt{R^2 - h^2}}{\Delta W dt} \quad (2.2)$$

Thus, the net-fraction of Type 2 collisions would be:

$$\frac{BC}{AC} = \frac{1}{\pi R^2} \int_{h_1}^R \frac{\Delta W dt - 2\sqrt{R^2 - h^2}}{\Delta W dt} 2\pi h dh \quad (2.3)$$

$$\frac{BC}{AC} = \frac{1}{3} \left(\frac{\Delta W dt}{2R} \right)^2 \dots\dots\text{if} \left(\frac{\Delta W dt}{2R} \right) \leq 1$$

and,

$$\frac{BC}{AC} = 1 - \frac{2}{3} \frac{1}{\Delta W dt/2R} \dots\dots\text{if} \left(\frac{\Delta W dt}{2R} \right) > 1$$

when

$$\left(\frac{\Delta W dt}{2R} \right) = 1, \frac{BC}{AC} = 1/3$$

Figure 2.5 shows a comparison of the predicted percentage of Type 2 collisions with actual simulation results. The agreement of our simulation results with the theoretical prediction shows a good validation for the collision detection scheme used in the code.

2.1.3 Pair and collision statistics

Before we go into the statistics of the collisions, we define some important pair statistics.

Radial relative velocity: It is defined in terms of the relative velocity \mathbf{w} , between two droplets with separation vector \mathbf{r} , as $w_r = \mathbf{w} \cdot \mathbf{r}/|\mathbf{r}|$, with $\mathbf{r} = |\mathbf{r}|$. The average radial relative velocity at contact, represents the average relative flux on the geometric collision sphere if particles are uniformly distributed.

Radial distribution function (RDF): The RDF is defined as the ratio of the actual pair density realized in a region (spherical shell in this case, as shown in figure 2.6) to the expected pair density in a uniform droplet distribution. Blue balls are particles at contact. Red line is the sphere with diameter R , where R is the separation

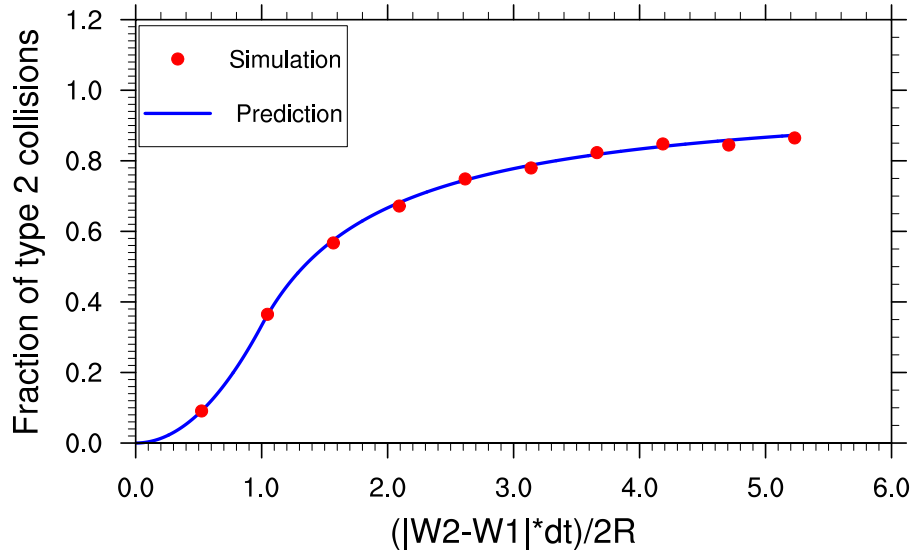


Figure 2.5: Comparison of theory and simulation for type 2 collisions

distance. Distance between red and pink lines, and distance between red and orange lines are the shell thickness (usually 2% of R). It is denoted by $g(r)$. For uniform distribution $g(r) = 1$.

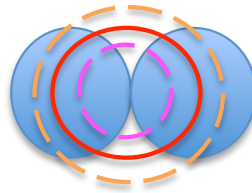


Figure 2.6: Spherical shell and RDF

Collision kernel: It is defined as the rate of collisions per unit volume, per average particle pair concentration. Formulation below is for bi-disperse case. It can be of two types, dynamic (collisions are counted as they occur), kinematic (collision kernel

is calculated based on relative velocity in radial direction and the radial distribution function). The dynamic collision kernel is given by:

$$\Gamma_{12} = \frac{\dot{N}_c}{n_1 n_2} \quad (2.4)$$

and the kinematic collision kernel is given by:

$$\Gamma_{12} = 2\pi R^2 \langle w_r \rangle g(r) \quad (2.5)$$

where Γ_{12} is the collision kernel, \dot{N}_c is collision rate per unit volume, n_1 , n_2 , are the average particle number concentration for the respective particle size, w_r is the relative velocity in the radial direction and the angular brackets denote ensemble average (defined later), $g(r)$ is the radial distribution function, R is the geometric collision radius (Saffman and Turner, 1956, Sundaram and Collins, 1997, Wang et al. 1998a, Wang et al., 2008).

Collision efficiency: It is the ratio of collision kernel calculated by considering hydrodynamic interactions, to collision kernel calculated without considering hydrodynamic interactions. Since hydrodynamic interactions would prevent some collisions to occur, collision efficiency is usually less than 1.

Collision efficiency enhancement factor: It is the ratio of collision efficiency in a turbulent flow to collision efficiency in a gravity only case (still fluid sedimentation). This quantity depicts the effect of turbulence on the collision efficiency.

$$E = \frac{\eta_T}{\eta_G} = \frac{\Gamma_{HI}^T / \Gamma_{NHI}^T}{\Gamma_{HI}^G / \Gamma_{NHI}^G} \quad (2.6)$$

where E is the collision efficiency enhancement factor, η is the collision efficiency, Γ is the collision kernel, subscript HI and NHI refer to with and without considering hydrodynamic interactions, respectively and superscript T , and G , refer to turbulent flow, and gravity only (still fluid sedimentation), respectively.

2.1.4 Uncertainty analysis for collision kernel: gravity only case

For the uncertainty analysis of gravity only case, we consider the gravity only case to be a special case of turbulent flow case, (i.e. with dissipation rate = 0). Below

are some input parameters for our simulation of gravity only flow (for particle sizes 30 and 40 μm in cloud units), All units below have been converted to DNS units, for example:

$L_b = 2\pi$ in DNS units, and L_b/η should be constant in both cloud units as well as DNS units, thus,

$$\frac{L_{b,DNS}}{\eta_{DNS}} = \frac{L_{b,cloud}}{\eta_{cloud}}$$

It should be noted that in gravity only case there is no flow, so for the DNS setting of Kolmogorov parameters, we chose $100 \text{ cm}^2/\text{s}^3$ as the dissipation rate. Basically the Stokes number (St), non-dimensional settling velocity (Sv), and ratio of radius to Kolmogorov length scale (r/η) are constant in both units, and based on these relations, the conversion of a quantity between DNS and cloud units are performed.

Domain size: $L_b = 2\pi = 6.283$

Differential sedimentation velocity: $\Delta W = 19.102$

Particle number in each group: $N_1 = N_2 = 145075$

$\Delta t = L_b/\Delta W = 0.328911$

Discretization time step size: $dt = 0.0001$

Total number of time-steps: $\Delta t/dt = 3289.11 \sim 3290$

Resolution: 128^3

First we determine the uncertainty for collision kernel. If we use the total number of time-steps to be less than $\Delta t/dt = 3289.11$, then we will miss out on some collisions. After every $\Delta t/dt = 3289.11$, the entire phenomenon repeats itself. Also, we are performing two averages, one is over the time-steps for each realization, and another is over multiple realization. For the standard deviation of a single realization, we use

$$SD = \sqrt{\frac{1}{N} \sum_{i=1}^N (\Gamma_i - \Gamma_{mean})^2} \quad (2.7)$$

where SD is the standard deviation for a single realization, N is the number of time-steps, Γ_i collision kernel in each time-step, and Γ_{mean} is the mean collision kernel over all the time-steps.

For multiple realizations, we need to calculate the standard deviation of the mean, in order to do that we use time correlation analysis, as we know that the collision events in gravity only case has complete correlation after every $\Delta t = L_b/\Delta W$. We use the following equation (Bendat J., Piersol A., Wiley. 2010)

$$\sigma_{mean}^2 = \frac{\sigma^2}{N} + 2\frac{\sigma^2}{N^2} \sum_{m=1}^{N-1} (N-m) R(m) \quad (2.8)$$

where σ_{mean} is the standard deviation of the mean, σ is the standard deviation of each realization, N is the total number of time-steps in all realizations, m is the time-lag, and R is the auto-correlation function. For complete correlation, $R(m) = 1$, for no correlation, $R(m) = 0$.

Let us consider $S = \Delta t/dt$, in our simulations S is not an exact integer, however, for simplicity of the derivation below we consider S to be exact integer. So, according to the above definition of the autocorrelation function R , $R(0) = 1$, $R(S) = 1$, $R(2S) = 1$..., and so on. All others should be zero, as the collisions are not correlated with in the time $\Delta t = L_b/\Delta W$. We can say, that we run the simulation for $N = kS$ time steps, where k is an integer, which means, equation 2.8 reduces to:

$$\sigma_{mean}^2 = \frac{\sigma^2}{N} + 2\frac{\sigma^2}{N^2} [(N-S) + (N-2S) + \dots + (N-(k-1)S)]$$

or,

$$\sigma_{mean}^2 = \frac{\sigma^2}{N} + 2\frac{\sigma^2}{N^2} \left[\frac{k-1}{2} (N-S + N-(k-1)S) \right]$$

or,

$$\sigma_{mean}^2 = \frac{\sigma^2}{N} + \frac{\sigma^2}{N^2} (k-1) (2N - kS)$$

or,

$$\sigma_{mean}^2 = \frac{\sigma^2}{kS} + \frac{\sigma^2}{kS} (k-1)$$

or,

$$\sigma_{mean}^2 = \frac{\sigma^2}{S} \quad (2.9)$$

A validation of this equation is given in figure 2.7, where we plot the auto-correlation function as a function of the time-lag, $m = 5 * dt$. The spikes in the plot are after every Δt , the reason for all the spikes not being exactly 1, is that the ratio of $\Delta t/dt$ is not an exact integer. This validates our formulation for standard deviation in the gravity only case.

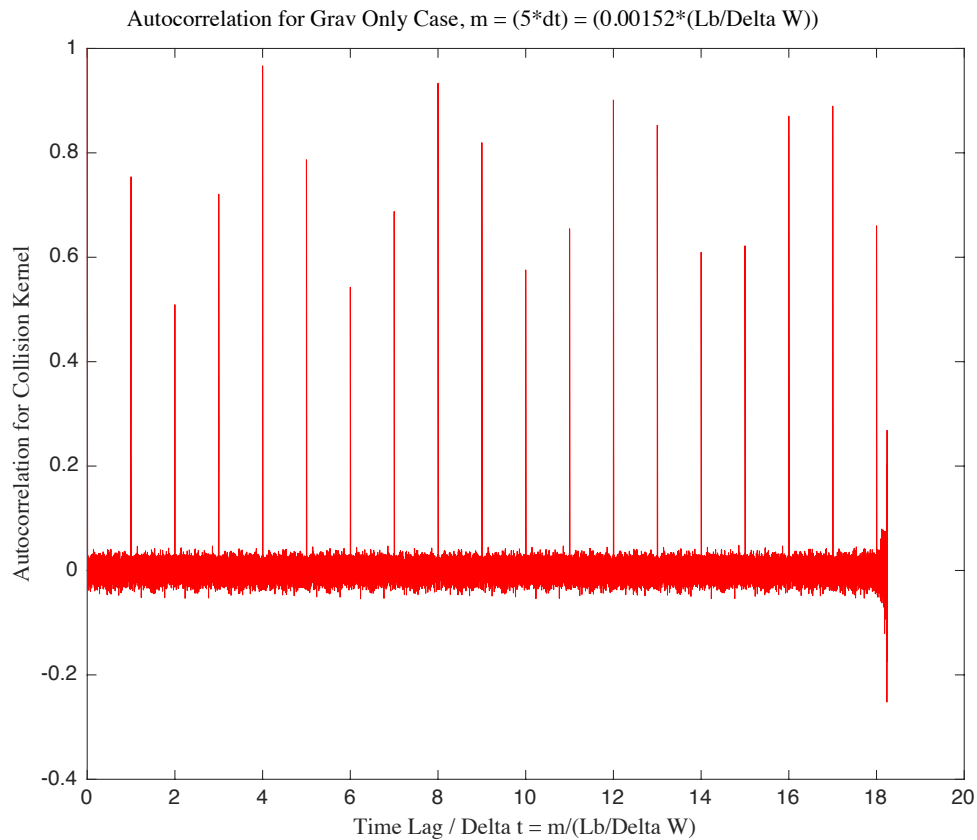


Figure 2.7: Auto-Correlation for gravity only

2.1.5 Results for collision kernel: gravity only case

For gravity only case without considering hydrodynamic interactions (i.e. NOHI), we compare our collision kernel results with the theoretical value. Table 2.1 shows the results for 30-40 μm radius particles, with 128^3 resolution, and for 22 different realizations of particle initial position configuration:

Table 2.1: Collision kernel with standard deviation for 30-40 μm radius particles for gravity only and NoHI case

No. of Realization	Collision kernel	Standard Deviation
1	1.37242E-03	1.87613E-05
2	1.35948E-03	1.85021E-05
3	1.36484E-03	1.84053E-05
4	1.42359E-03	1.84545E-05
5	1.39064E-03	1.86959E-05
6	1.36203E-03	1.81304E-05
7	1.37019E-03	1.82984E-05
8	1.37209E-03	1.85016E-05
9	1.39014E-03	1.86940E-05
10	1.34992E-03	1.77185E-05
11	1.40381E-03	1.89677E-05
12	1.35363E-03	1.80519E-05
13	1.38750E-03	1.86468E-05
14	1.38198E-03	1.89628E-05
15	1.36722E-03	1.84918E-05
16	1.39583E-03	1.87434E-05
17	1.36203E-03	1.81843E-05
18	1.40258E-03	1.84982E-05
19	1.34472E-03	1.83299E-05
20	1.38329E-03	1.82541E-05
21	1.40357E-03	1.84125E-05
22	1.40827E-03	1.83248E-05
Mean (Simulations)	1.37954E-03	3.93530E-06
Theoretical	1.38089E-03	-

Different realizations show different collision kernels, which is expected as the initial position configuration is different for the particle. The difference between the

theoretical result and the mean value over 22 realizations for our simulation is less than 1% (which is within the standard deviation of the mean), which shows that our results are correct. An example schematic of two different position configurations is shown in figure 2.8, which explains why collision kernel should differ for two different configurations. The first case shows an initial position in which the particles will definitely collide, but in the second case, the particles will fail to collide as we allow particles to overlap in the gravity only case. However, if we consider hydrodynamic interactions among the particles (hence do not allow particles to overlap) or include a turbulent flow instead of still fluid, then this initial position bias would be removed over time, as there would be a horizontal component of velocity acting.

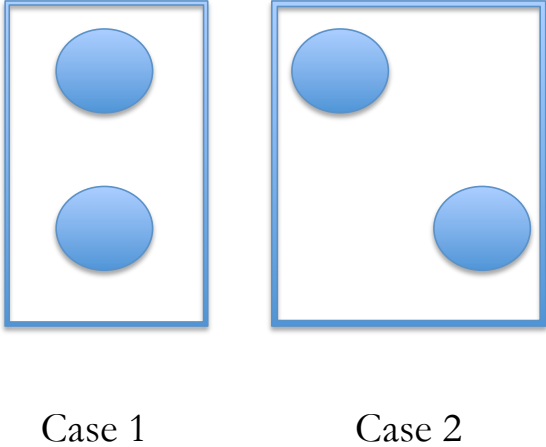


Figure 2.8: Initial position bias

2.1.6 Collision statistics for gravity only with hydrodynamic interactions

When considering hydrodynamic interactions, in stagnant fluid the the disturbance flow due to the particle may extend up to 50 times the droplet radius (Lin and Lee 1975, 1976). The droplet disturbance flow does not affect the mean fluid flow, but

it affects the motion of other particles, for particles close to the concerned droplet, the effect of background flow would be higher, and the effect decreases with increasing distance between two particles. The largest distance which can have some effect is on the order of the Kolmogorov length scale of the turbulence (or smaller), for distances larger than this, the effect is negligible. We initially assume the disturbance flow due to the presence of a particle to be a Stokes flow. For particles in stagnant fluid, the equation for the disturbance flow becomes:

$$u_r = \left[\frac{3}{2} \frac{1}{r} - \frac{1}{2} \left(\frac{a}{r} \right)^3 \right] v_p \cos \theta \quad (2.10)$$

$$u_\theta = \left[\frac{3}{4} \frac{1}{r} + \frac{1}{4} \left(\frac{a}{r} \right)^3 \right] (-v_p \sin \theta) \quad (2.11)$$

$$u_\phi = 0 \quad (2.12)$$

Wang et al. 2005b, presented a formulation for a system of arbitrary particles. The disturbance velocity felt by a given particle is given by:

$$\vec{u}^{(k)} = \sum_{m=1}^{N_p} \vec{u}_s(\vec{Y}^{(k)}(t) - \vec{Y}^{(m)}(t); a^{(m)}, \vec{V}^{(m)} - \vec{U}(\vec{Y}^{(m)}, t) - \vec{u}^{(m)}) \dots k = 1, 2 \dots N_p, \text{ and } m \neq k \quad (2.13)$$

where Stokes disturbance flow induced by k^{th} droplet is:

$$u_s(\vec{r}^{(k)}; a^{(k)}, \vec{V}_p^{(k)}) = \left[\frac{3}{4} \frac{a^{(k)}}{r^{(k)}} - \frac{3}{4} \left(\frac{a^{(k)}}{r^{(k)}} \right)^3 \right] \frac{\vec{r}^{(k)}}{(r^{(k)})^2} \left(\vec{V}_p^{(k)} \cdot \vec{r}^{(k)} \right) + \left[\frac{3}{4} \frac{a^{(k)}}{r^{(k)}} + \frac{1}{4} \left(\frac{a^{(k)}}{r^{(k)}} \right)^3 \right] \vec{V}_p^{(k)} \quad (2.14)$$

Once the disturbance flow velocities are computed at all droplet locations, the droplets are advanced by solving the equation of motion. The equation of motion for k^{th} droplet is:

$$\frac{d\vec{V}^{(k)}(t)}{dt} = - \frac{\vec{V}^{(k)}(t) - (\vec{U}(\vec{Y}^{(k)}(t), t) + \vec{u}^{(k)})}{\tau_p^{(k)}} + \vec{g} \quad (2.15)$$

and

$$\frac{d\vec{Y}^{(k)}(t)}{dt} = \vec{V}^{(k)}(t) \quad (2.16)$$

When we consider hydrodynamic interaction effect, we do not allow the particles to overlap, as soon as the particles collide, we withdraw the colliding particles from the system, and re-introduce them at two random positions. A brief explanation of the hydrodynamic interactions is presented here. Ayala et al., 2007 provides the description in detail.

Collision kernel results with HI case is given in table 2.2. The collision kernel with HI case is lower than that of the NoHI case, which makes sense as the pressure difference due to the presence of fluid between two particles will try to push the particles away, and hence prevents some of the collisions, resulting in a lower collision kernel.

Table 2.2: Collision kernel with standard deviation for 30-40 μm radius particles for gravity only and with HI case

No. of Realization	Collision kernel	Standard Deviation
1	9.79755E-04	1.58991E-05
2	9.97359E-04	1.56019E-05
3	1.03075E-03	1.57956E-05
4	1.01188E-03	1.60247249E-05
5	1.01664E-03	1.59905413E-05
6	1.01120E-03	1.60151078E-05
7	1.02622E-03	1.61512291E-05
8	9.91480E-04	1.56939892E-05
9	9.97303E-04	1.54912429E-05
10	9.78766E-04	1.54463340E-05
11	1.00521E-03	1.59252505E-05
12	9.86286E-04	1.52072212E-05
13	9.83462E-04	1.59160647E-05
14	1.03260E-03	1.57080097E-05
15	9.89394E-04	1.51688214E-05
16	9.83709E-04	1.54339352E-05
17	9.85544E-04	1.54827973E-05
18	1.01905E-03	1.58494924E-05
19	9.95134E-04	1.53910660E-05
20	9.92167E-04	1.59935327E-05
21	1.01682E-03	1.58408810E-05
22	1.01553E-03	1.55686701E-05
Mean	1.0021E-03	3.3496E-06

Collision efficiency results are presented in the table 2.3

Table 2.3: Collision efficiency with standard deviation for 30-40 μm radius particles for gravity only

Case	Collision Efficiency	Standard Deviation
Simulations	0.72640	3.19209E-03
Code for published results*	0.71875	-

where the standard deviation is calculated by the equation:

$$sd_E = \frac{\Gamma_{HI}}{\Gamma_{NHI}} \sqrt{\frac{(sd_{\Gamma_{HI}})^2}{\Gamma_{HI}^2} + \frac{(sd_{\Gamma_{NHI}})^2}{\Gamma_{NHI}^2}} \quad (2.17)$$

where sd_E is the standard deviation for collision efficiency, Γ is the collision kernel, sd_{Γ} is the standard deviation for collision kernel, subscripts HI and NHI correspond to cases with hydrodynamic interactions and without hydrodynamic interactions, respectively.

*Published results for collision efficiency of 30-40 μm radii particle-pair were not available in the literature, however we used the exact same code to generate the results for 30-40 μm radii particle-pair as were used by Wang et al. 2005. The published results in Wang et al. 2005 are for different particle sizes, however they used this same code to generate those results. The percentage difference between our results and Wang et al. is about 1%.

2.2 Collision Statistics In Turbulent Flow

For the turbulent flow, we generate the fluid turbulence using a pseudo-spectral method in a periodic domain, using the Navier-Stokes equation:

$$\frac{\partial \vec{U}}{\partial t} = \vec{U} \times \omega - \nabla \left(\frac{P}{\rho} + \frac{1}{2} \vec{U}^2 \right) + \nu \nabla^2 \vec{U} + \vec{f}(\vec{x}, t) \quad (2.18)$$

and the continuity equation:

$$\nabla \cdot \vec{U}(\vec{x}, t) = 0 \quad (2.19)$$

where \vec{U} is the flow-field $\omega = \nabla \times \vec{U}$ is the vorticity, P is the pressure, ρ is the fluid density, and ν is the air kinematic viscosity.

We perform simulations at specific flow dissipation rates. For this thesis we typically use dissipation rates of $\epsilon = 100, 30, 10, 3 \text{ cm}^2/\text{sec}^3$, as this range is specific to stratocumulus clouds. Details of the method for the flow simulation have been presented in Wang and Maxey, 1993 and Wang et al. 2000.

For low dissipation rates, like $3 \text{ cm}^2/\text{sec}^3$, we need multiple realizations as the turbulence is weak, which means that the particle motion is heavily driven by gravity.

2.2.1 Uncertainty for collision kernel in turbulent flow case

We use the same equation, as in the gravity only case for the uncertainty given by equation 2.8, namely:

$$\sigma_{mean}^2 = \frac{\sigma^2}{N} + 2 \frac{\sigma^2}{N^2} \sum_{m=1}^{N-1} (N-m) R(m)$$

For the gravity only case, we know that the collision events were completely correlated after every $L_b/\Delta W$, however, in a turbulent flow there is no such correlation. But, in a turbulent flow we do know that the flow has a correlation time scale known as the integral time scale, we need to check if the collision events are correlated in that time. In order to do that we need to calculate the auto-correlation function between the collision events. We expect the correlation between the collision events to be very small (~ 0), as the collision events are taking place in a different place in that small amount of time.

The auto-correlation function is given as:

$$R(m) = \frac{1}{(N-m)\sigma^2} \sum_{i=1}^{N-m} (X_i^j - \mu) (X_{i+m}^j - \mu) \quad (2.20)$$

where μ is the mean, σ is the standard deviation and X is the variable for which we are calculating the auto-correlation function, i.e. the correlation with itself at a later time. The integral time scale is given as:

$$T_{int} = \int_0^{\infty} R(m)dm \quad (2.21)$$

The auto-correlation function for dissipation rate of $10cm^2/sec^3$ is shown in figure 2.9. The *Deltat* mentioned in the figure is $\Delta t = L_b/\Delta W$.

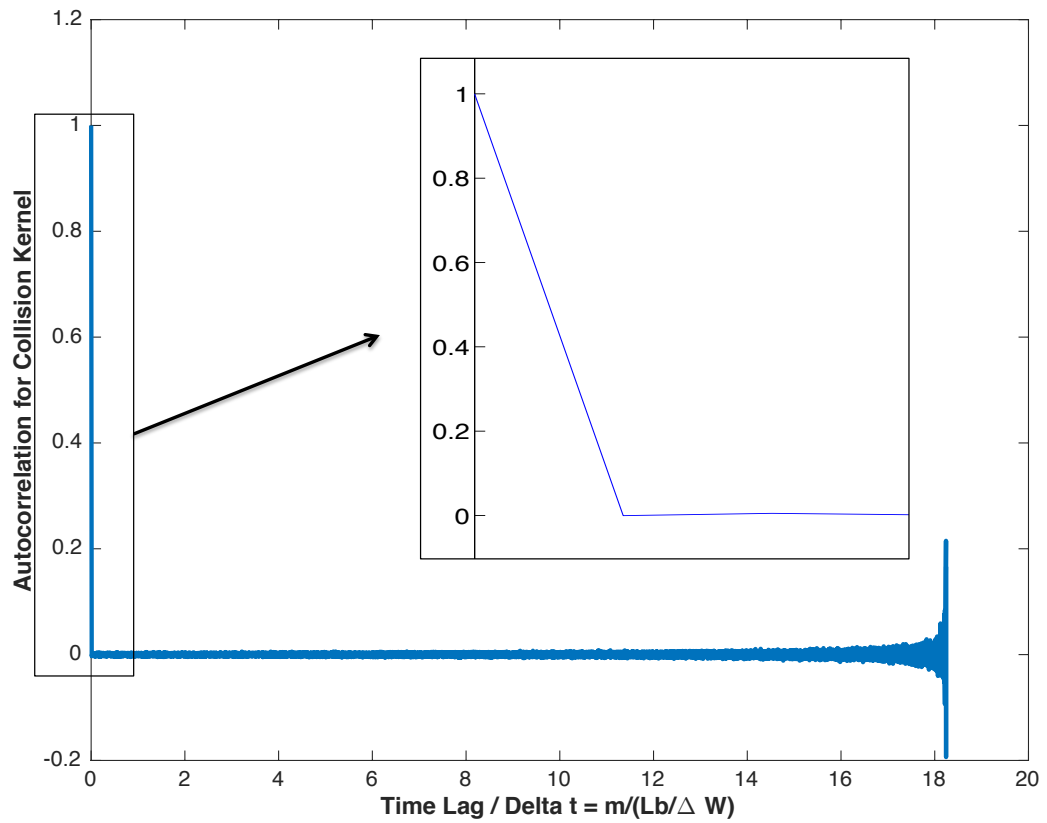


Figure 2.9: Auto-Correlation for dissipation rate of $10cm^2/sec^3$; Here $m = (5 * dt)$, so $m/Deltat = (0.00152/(L_b/\Delta W))$

A zoomed in box, shows that at $m = 0$, the auto-correlation is 1, which is correct because at any given time, the variable will be same. But, at the very next step, we see that the auto-correlation function drops to 0, which backs our hypothesis. We see similar results for dissipation rates 30 and 100 cm^2/sec^3 as well. This shows that the collision events are un-correlated temporally.

To check our hypothesis for the spatial correlation, that the collision events in a turbulent flow are un-correlated, we remove the particles from the system as soon as they collide even for the NoHI case. By doing this, we should not see a drop in the collision kernel as per our hypothesis. If the collisions were indeed correlated, then removal of those particles would result in the collision kernel, as the correlated collisions are not occurring.

Table 2.4 shows the comparison of the two collision kernels for NoHI but with and without removal of particles after collision for 30 – 40 μm particle radius, and 100 cm^2/sec^3 dissipation rate , each of the results were obtained after averaging over 12 realizations.

Table 2.4: Collision kernel with standard deviation comparison for dissipation rate 100 cm^2/sec^3

Case	Collision Kernel	Standard Deviation
No-removal	1.5413E-03	5.92E-07
With-removal	1.5414E-03	5.96E-07

This shows that the collision events are not correlated either temporally or spatially in a turbulent flow. For,

$$\sigma_{mean}^2 = 2\sigma^2 \frac{T_{int}}{T}$$

to be true, we need $dt \ll 2 * T_{int}$ If we consider a very small dt , then we will have either 0 or 1 collision in each time-step. The smaller it is, more zeros we will get, so the mean

value of the number of collisions will be close to 0 ($\mu \sim 0$). Thus the auto-correlation function for any value of m will become:

$$\text{For } X_i = 0 : X_{i+m} = 0 \rightarrow (0 - 0)(0 - 0) = 0$$

$$\text{For } X_i = 0 : X_{i+m} = 1 \rightarrow (0 - 0)(1 - 0) = 0$$

$$\text{For } X_i = 1 : X_{i+m} = 0 \rightarrow (1 - 0)(0 - 0) = 0$$

$$\text{For } X_i = 1 : X_{i+m} = 1 \rightarrow (1 - 0)(1 - 0) = 1$$

Due to the very small dt , we will get a lot more zeros, so we can conclude that $R(i) \sim 0$, and T_{int} would be very small.

Since the auto-correlation function becomes 0, the equation for calculating the variance of the mean collision kernel for multiple realizations in the turbulent flow case becomes:

$$\sigma_{mean}^2 = \frac{\sigma^2}{N} \tag{2.22}$$

where N is the total number of time-steps combined in all realizations.

2.2.2 Collision kernel results in a turbulent flow

Collision kernel results for dissipation rate of $3cm^2/sec^3$ are given in the table 2.5, it should be noted that this case is run for a time of $L_b/\Delta W$:

Table 2.5: Collision kernel with standard deviation for 30-40 μm radius particles for dissipation rate $3\text{cm}^2/\text{sec}^3$

	NoHI		With HI	
Realization	Collision Kernel	SD	Collision Kernel	SD
1	1.38535E-03	2.09085E-06	1.02158E-03	1.78274E-06
2	1.38685E-03	2.05023E-06	1.02139E-03	1.75096E-06
3	1.38913E-03	2.08296E-06	1.02111E-03	1.77678E-06
4	1.38409E-03	2.09084E-06	1.02461E-03	1.75038E-06
5	1.38726E-03	2.06759E-06	1.02459E-03	1.77905E-06
6	1.38679E-03	2.07339E-06	1.02293E-03	1.77975E-06
7	1.38406E-03	2.06425E-06	1.02183E-03	1.78024E-06
8	1.38833E-03	2.06557E-06	1.02421E-03	1.77172E-06
9	1.38585E-03	2.06939E-06	1.01933E-03	1.78161E-06
10	1.38588E-03	2.06344E-06	1.02328E-03	1.78280E-06
Mean	1.38636E-03	6.55189E-07	1.02249E-03	5.60876E-07

Collision kernel results with standard deviation for dissipation rate of $10\text{cm}^2/\text{sec}^3$ are given in the table 2.6, it should be noted that this case is run for a time of $L_b/\Delta W$:

Table 2.6: Collision kernel with standard deviation for 30-40 μm radius particles for dissipation rate $10cm^2/sec^3$

	NoHI		With HI	
Realization	Collision Kernel	SD	Collision Kernel	SD
1	1.39855E-03	4.31851E-06	1.03703E-03	3.84425E-06
2	1.39935E-03	4.41484E-06	1.03639E-03	3.83789E-06
3	1.39993E-03	4.35920E-06	1.03509E-03	3.83103E-06
4	1.39924E-03	4.40412E-06	1.03651E-03	3.84587E-06
5	1.39842E-03	4.42582E-06	1.03645E-03	3.74997E-06
Mean	1.39910E-03	1.96089E-06	1.03629E-03	1.70924E-06

Collision kernel results with standard deviation for dissipation rate of $30cm^2/sec^3$ are given in the table 2.7, it should be noted that this case is run for about $45 \times L_b/\Delta W$:

Table 2.7: Collision kernel with standard deviation for 30-40 μm radius particles for dissipation rate $30cm^2/sec^3$

	NoHI		With HI	
Realization	Collision Kernel	SD	Collision Kernel	SD
1	1.43719E-03	1.48594E-06	1.07132E-03	1.25094E-06
2	1.43501E-03	1.47288E-06	1.07623E-03	1.27743E-06
3	1.43444E-03	1.46163E-06	1.07599E-03	1.28067E-06
4	1.43594E-03	1.47561E-06	1.07521E-03	1.27950E-06
5	1.43348E-03	1.45475E-06	1.07521E-03	1.27384E-06
Mean	1.43521E-03	6.57495E-07	1.07479E-03	5.69090E-07

Collision kernel results with standard deviation for dissipation rate of $100\text{cm}^2/\text{sec}^3$ are given in the table 2.8, it should be noted that this case is run for about than $45 \times L_b/\Delta W$:

Table 2.8: Collision kernel with standard deviation for 30-40 μm radius particles for dissipation rate $100\text{cm}^2/\text{sec}^3$

	NoHI		With HI	
Realization	Collision Kernel	SD	Collision Kernel	SD
1	1.53791E-03	3.20733E-06	1.18187E-03	2.82686E-06
2	1.54298E-03	3.23359E-06	1.18511E-03	2.83801E-06
3	1.54648E-03	3.25160E-06	1.18872E-03	2.84624E-06
4	1.54485E-03	3.23715E-06	1.18164E-03	2.82472E-06
Mean	1.54305E-03	1.61623E-06	1.18429E-03	1.26769E-06

From the above results, it is clear that the collision kernel increases with dissipation rate, which agrees with the known fact that turbulence increases collision kernel.

2.2.3 Collision efficiency and collision efficiency enhancement

Table 2.9 provides the results of collision efficiency in a turbulent flow for different dissipation rates. We also include the collision efficiency for the gravity only case in the table to compare the results. The standard deviations of the mean value of collision efficiency is provided with in brackets.

Table 2.9: Collision efficiency with standard deviation for 30-40 μm radius particles in turbulent flow

No. of Realizations	Dissipation Rate(cm^2/sec^3)	Collision Efficiency (SD)
22	0(Gravity only)	0.726(3.19E-03)
10	3	0.737(3.60E-04)
5	10	0.740(1.6E-03)
5	30	0.748(5.24E-04)
4	100	0.767(1.14E-03)

The results agree with the fact that collision efficiency increases with turbulence, as we see that the collision efficiency becomes higher with an increase in turbulence dissipation rate.

Next we take a look at the collision efficiency enhancement factor. Previously it was assumed that the collision efficiency enhancement factor increases linearly with increasing dissipation rate, due to lack of DNS data. As the cases of low dissipation rates are expensive to simulate, a linear interpolation model is generally followed to determine the collision efficiency at low dissipation rates. However, we find a non-linear behavior in our results. Figure 2.10 shows the comparison of enhancement factor at different dissipation rates.

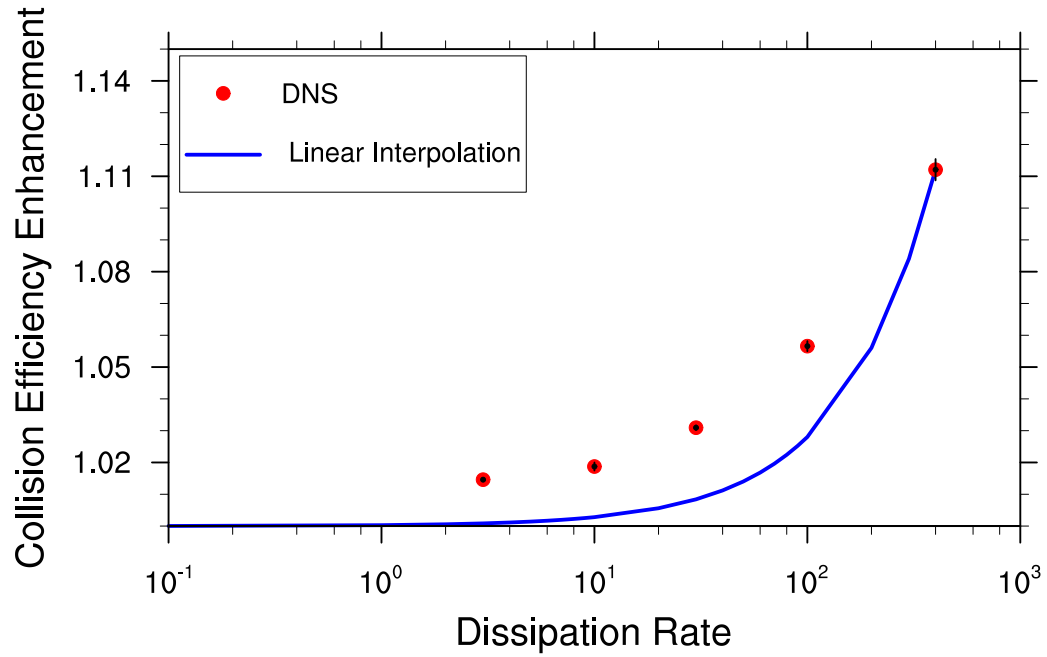


Figure 2.10: Comparison of collision efficiency enhancement with linear interpolation

This non-linearity could be arising due to the coupling of the turbulence and hydrodynamic interactions. Further studies are required to determine the reason behind it, this could be a possible direction for future work.

Chapter 3

ASYMPTOTIC EXPANSION APPROACH FOR PARTICLE TRACKING

3.1 Motivation & Background

Asymptotic expansion approach provides an approximation for the local instantaneous velocity of small inertia particles. It was briefly mentioned in Chapters 1 & 2, that for cases with low flow dissipation rates ($1 \sim 30 \text{cm}^2/\text{s}^3$) the particle Stokes number tends to be low and the simulations become very expensive. This is the primary motivation for the implementation of the asymptotic expansion approach (details about the motivation are described in subsequent sections in this chapter) which was first used by Maxey 1987 in a 2-D cellular flow. In this chapter, we first discuss the details of the motivation, for implementing this approach, next we provide a derivation of the equation, then we validate our implementation using a 2-D cellular flow, as in Maxey 1987, finally we compare results of the asymptotic approach with the direct integration approach which we have been using so far.

For strato-cumulus clouds, as mentioned earlier, the dissipation rates are relatively lower than that of cumulus clouds (typically less than $100 \text{cm}^2/\text{s}^3$), also the droplet size range in strato-cumulus clouds is relatively smaller (typically $5 - 40 \mu\text{m}$). Since the CFL condition determines the numerical stability of the spectral simulation of the turbulent flow, we start from that to determine why the simulations are expensive, when we have a combination of low particle Stokes number and low flow dissipation rate. The CFL number is defined as:

$$CFL = \frac{U_{max} dt_{flow}}{dx} \quad (3.1)$$

where U_{max} is the maximum flow velocity, dt is the discretization time-step size, and dx is the distance between two adjacent grid locations in a given spatial direction.

As an estimate we set $U_{max} \sim 5u'$, where u' is the r.m.s. fluctuation velocity, and in the spectral method for air turbulence simulation, generally, $dx = 2\eta$, where η is the Kolmogorov length scale. In Direct Numerical Simulations (DNS), the CFL number is typically less than 0.25. So, dt becomes:

$$dt_{flow} \sim 0.25 \frac{2\eta}{5u'} \quad (3.2)$$

or,

$$dt_{flow} \sim \frac{1}{10} \frac{\eta}{u'}$$

or,

$$\frac{dt_{flow}}{\tau_k} \sim \frac{1}{10} \frac{\eta}{u'\tau_k}$$

or,

$$\frac{dt_{flow}}{\tau_k} \sim \frac{1}{10} \frac{v_k}{u'} \quad (3.3)$$

where τ_k and v_k are the Kolmogorov time scale and Kolmogorov velocity scale, respectively. Equation 3.3 can be alternatively written as:

$$dt_{flow} = CFL \times \frac{2}{5} 15^{0.25} Re_\lambda^{-0.5} \sqrt{\frac{\nu}{\epsilon}} \quad (3.4)$$

where Re_λ is the Taylor micro-scale Reynolds number, ν is the flow viscosity (air in this case), and ϵ is the average flow dissipation rate. Since we have particle motion involved in this problem, the particle inertial response time, τ_p is an important dynamic time-scale of the problem. The particle response time is given by the equation:

$$\tau_p = \frac{2}{9} \frac{\rho_w}{\rho} \left(\frac{a}{\eta} \right)^2 \tau_k \quad (3.5)$$

Combining equations 3.4 and 3.5, we obtain:

$$\frac{dt_{flow}}{\tau_p} = \frac{0.8 \times CFL \times \nu^{1.5}}{\sqrt{Re_\lambda} \times \frac{2}{9} \times 1000 \times a^2 \times \sqrt{\epsilon}} \quad (3.6)$$

Equation 3.6, shows that as the average flow dissipation rate ϵ , and the particle radius, a are reduced, the particle inertial response time τ_p may become smaller than the time

step dt_{flow} needed for the flow simulation. Since the time step for integrating the particle velocity must be less than τ_p , then in this case, the time step size is governed by τ_p . So for low dissipation rates and small particle radius, as in the case of strato-cumulus clouds the dt required is very small. Hence we need to run the simulations for comparatively more time steps to obtain reasonable average statistics with small uncertainty, making the simulations computationally very expensive.

3.2 The Asymptotic Expansion

Here we provide a general procedure to obtain asymptotic expressions for local velocity of small-inertia particles. The method starts with the formal integral formulation of the equation of motion for a small heavy particle:

$$\tau_p \frac{dV_i(t, \mathbf{Y}_0, \mathbf{V}_0)}{dt} = [u_i(\mathbf{Y}, t) - V_i + W_i^S] \quad (3.7)$$

$$\frac{dY_i(t, \mathbf{Y}_0, \mathbf{V}_0)}{dt} = V_i(t, \mathbf{Y}_0, \mathbf{V}_0) \quad (3.8)$$

where, τ_p is the particle inertial response time, $V_i(t)$ is the particle velocity, $u_i(\mathbf{x}, t)$ is the flow field, and W_i^S is the *constant* particle settling velocity in still fluid. \mathbf{Y}_0 and \mathbf{V}_0 are particle initial position and initial velocity at $t = 0$. Equation 3.7 can be re-written as:

$$\tau_p \frac{dV_i}{dt} + V_i = u_i(Y_i(t, \mathbf{Y}_0, \mathbf{V}_0), t) + W_i^S \quad (3.9)$$

The solution of the differential Eq. (3.9) can be written as:

$$V_i(t, \mathbf{Y}_0, \mathbf{V}_0) = S_i(t, \mathbf{Y}_0, \mathbf{V}_0) e^{-\frac{t}{\tau_p}} \quad (3.10)$$

where, S_i is an arbitrary function of t . So, for initial condition at $t = 0$, we have:

$$S_i(t = 0, \mathbf{Y}_0, \mathbf{V}_0) = V_{0i} \quad (3.11)$$

Thus, we have:

$$\frac{dS_i}{dt} = \frac{1}{\tau_p} [u_i(Y(t, \mathbf{Y}_0, \mathbf{V}_0), t) + W_i^S] e^{\frac{t}{\tau_p}} \quad (3.12)$$

Integrating, we obtain

$$S_i(t, \mathbf{Y}_0, \mathbf{V}_0) = V_{0i} + \int_0^t \frac{1}{\tau_p} [u_i(Y(\theta, \mathbf{Y}_0, \mathbf{V}_0), \theta) + W_i^S] e^{\frac{\theta}{\tau_p}} d\theta \quad (3.13)$$

which yields that,

$$V_i(t, \mathbf{Y}_0, \mathbf{V}_0) = e^{-\frac{t}{\tau_p}} \left\{ V_{0i} + \int_0^t \frac{1}{\tau_p} [u_i(Y(\theta, \mathbf{Y}_0, \mathbf{V}_0), \theta) + W_i^S] e^{\frac{\theta}{\tau_p}} d\theta \right\} \quad (3.14)$$

or,

$$V_i(t, \mathbf{Y}_0, \mathbf{V}_0) = V_{0i} e^{-t/\tau_p} + W_i^S (1 - e^{-t/\tau_p}) + \int_0^t u_i(Y(\theta, \mathbf{Y}_0, \mathbf{V}_0), \theta) e^{\left(-\frac{t-\theta}{\tau_p}\right)} \frac{d\theta}{\tau_p} \quad (3.15)$$

Now, at finite t , if we let $\tau_p \rightarrow 0$

$$V_i(t, \mathbf{Y}_0, \mathbf{V}_0) = W_i^S - \int_0^t u_i(Y(\theta, \mathbf{Y}_0, \mathbf{V}_0), \theta) e^{\left(-\frac{t-\theta}{\tau_p}\right)} d\left(\frac{t-\theta}{\tau_p}\right) \quad (3.16)$$

Let $\phi = (t - \theta)/\tau_p$, then $\theta = t - \tau_p \phi = t$.

$$V_i(t, \mathbf{Y}_0, \mathbf{V}_0) = W_i^S - u_i(\mathbf{Y}(t, \mathbf{Y}_0, \mathbf{V}_0), t) \int_{\infty}^0 e^{-\phi} d\phi = W_i^S + u_i(\mathbf{Y}(t, \mathbf{Y}_0, \mathbf{V}_0), t) \quad (3.17)$$

Therefore, in this limit of $\tau_p \rightarrow 0$, we can uniquely define a particle velocity field, with $\mathbf{x} = \mathbf{Y}(t, \mathbf{Y}_0, \mathbf{V}_0)$, as

$$V_i(\mathbf{x}, t) = W_i^S + u_i(\mathbf{x}, t) \quad (3.18)$$

Next, we consider a small but finite τ_p . Starting from the general expression

$$V_i(t, \mathbf{Y}_0, \mathbf{V}_0) = V_{0i} e^{-t/\tau_p} + W_i^S (1 - e^{-t/\tau_p}) + \int_0^t u_i(Y(\theta, \mathbf{Y}_0, \mathbf{V}_0), \theta) e^{\left(-\frac{t-\theta}{\tau_p}\right)} \frac{d\theta}{\tau_p} \quad (3.19)$$

Now at finite t , small inertia limit, $\frac{\tau_p}{t} \ll 1$, or $\frac{t}{\tau_p} \gg 1$. Thus,

$$V_i(t, \mathbf{Y}_0, \mathbf{V}_0) = W_i^S + \int_0^t u_i(Y(\theta, \mathbf{Y}_0, \mathbf{V}_0), \theta) e^{\left(-\frac{t-\theta}{\tau_p}\right)} \frac{d\theta}{\tau_p} \quad (3.20)$$

The integral is contributed mainly by the small period $t - \delta \leq \theta \leq t$, and $\delta \sim \tau_p$.
Introducing

$$-\frac{t - \theta}{\tau_p} = q \rightarrow \theta = t + q\tau_p \quad (3.21)$$

Note that q is negative. We view that q is large in magnitude, but $-q\tau_p \ll t$, so we can then re-write the above expression as

$$V_i(t, \mathbf{Y}_0, \mathbf{V}_0) = W_i^S + \int_{-\infty}^0 u_i(\mathbf{Y}(t + \tau_p q, \mathbf{Y}_0, \mathbf{V}_0), t + \tau_p q) e^q dq \quad (3.22)$$

As, $-q\tau_p \ll t$, we can perform double Taylor expansion. We expand $u_i(\mathbf{Y}(t + \tau_p q, \mathbf{Y}_0, \mathbf{V}_0), t + \tau_p q)$, with respect to $q = 0$ and we set $\mathbf{x} \equiv \mathbf{Y}(t, \mathbf{Y}_0, \mathbf{V}_0)$.

$$\begin{aligned} u_i(\mathbf{Y}(t + \tau_p q, \mathbf{Y}_0, \mathbf{V}_0), t + \tau_p q) &= u_i(\mathbf{x}, t) \\ &+ \left(q\tau_p \frac{\partial}{\partial t} + [Y_j(t + q\tau_p, \mathbf{Y}_0, \mathbf{V}_0) - Y_j(t, \mathbf{Y}_0, \mathbf{V}_0)] \frac{\partial}{\partial x_j} \right) u_i \\ &+ \frac{1}{2} \left(q\tau_p \frac{\partial}{\partial t} + [Y_j(t + q\tau_p, \mathbf{Y}_0, \mathbf{V}_0) - Y_j(t, \mathbf{Y}_0, \mathbf{V}_0)] \frac{\partial}{\partial x_j} \right)^2 u_i \\ &+ \dots \end{aligned} \quad (3.23)$$

We know that

$$\frac{dY_i(t + q\tau_p; \mathbf{Y}(t) = \mathbf{x}, \mathbf{V}(t))}{d(q\tau_p)} = V_j(t + q\tau_p; \mathbf{Y}(t) = \mathbf{x}, \mathbf{V}(t)) \quad (3.24)$$

here t is a reference time, and we assume the particle will be located at \mathbf{x} with a velocity \mathbf{V} at time t .

Integrating from $(t + q\tau_p)$ to t , we have

$$Y_j(t; \mathbf{Y}(t) = \mathbf{x}, \mathbf{V}(t)) - Y_j(t + q\tau_p; \mathbf{Y}(t) = \mathbf{x}, \mathbf{V}(t)) = \tau_p \int_q^0 V(t + \zeta\tau_p; \mathbf{Y}(t), \mathbf{V}(t)) d\zeta \quad (3.25)$$

and expand the integrand as

$$V(t + \zeta\tau_p) = V(t) + \zeta\tau_p \frac{dV}{dt} + \frac{1}{2}(\zeta\tau_p)^2 \frac{d^2V}{dt^2} + \mathcal{O}(\tau_p^3), \quad (3.26)$$

where d/dt denotes the rate of change following the particle path at time t . Therefore

$$\begin{aligned}
Y_j(t, Y_0, V_0) - Y_j(t + q\tau_p, Y_0, V_0) &= \tau_p \int_q^0 \left[V(t) + \zeta \tau_p \frac{dV}{dt} + \frac{1}{2} (\zeta \tau_p)^2 \frac{d^2V}{dt^2} + \dots \right] d\zeta \\
&= -V(t) \tau_p q - \frac{\tau_p^2 q^2}{2} \frac{dV}{dt} - \frac{1}{6} \tau_p^3 q^3 \frac{d^2V}{dt^2} + \mathcal{O}(\tau_p^4)
\end{aligned} \tag{3.27}$$

Substituting Eq. 3.27 into Eq. 3.23, we can now write

$$\begin{aligned}
u_i(\mathbf{Y}(t + q\tau_p), t + q\tau_p; \text{given } \mathbf{Y}(t) = \mathbf{x}) \\
&= u_i(\mathbf{x}, t) \\
&+ \left(q\tau_p \frac{\partial}{\partial t} + \left[\tau_p q V_j(t) + \frac{1}{2} \tau_p^2 q^2 \frac{dV_j}{dt} + \frac{1}{6} \tau_p^3 q^3 \frac{d^2V_j}{dt^2} + \dots \right] \frac{\partial}{\partial x_j} \right) u_i \\
&+ \frac{1}{2} \left(q\tau_p \frac{\partial}{\partial t} + \left[\tau_p q V_j(t) + \frac{1}{2} \tau_p^2 q^2 \frac{dV_j}{dt} + \frac{1}{6} \tau_p^3 q^3 \frac{d^2V_j}{dt^2} + \dots \right] \frac{\partial}{\partial x_j} \right)^2 u_i + \dots
\end{aligned} \tag{3.28}$$

By ordering the terms in terms of τ_p , we have

$$\begin{aligned}
u_i(\mathbf{Y}(t + q\tau_p), t + q\tau_p; \mathbf{Y}(t) = \mathbf{x}) &= u_i(\mathbf{x}, t) + \tau_p \left(\frac{\partial u_i}{\partial t} + V_j(t) \frac{\partial u_i}{\partial x_j} \right) q \\
&+ \tau_p^2 \left[\frac{1}{2} \frac{dV_j}{dt} \frac{\partial u_i}{\partial x_j} + \frac{1}{2} \left(\frac{\partial}{\partial t} + V_j(t) \frac{\partial}{\partial x_j} \right)^2 u_i \right] q^2 + \mathcal{O}(\tau_p^3)
\end{aligned} \tag{3.29}$$

Inserting this into equation 3.22 we have

$$\begin{aligned}
V_i(t; \mathbf{Y}(t) = \mathbf{x}) &= W_i^S \\
&+ u_i(Y(t), t) \int_{-\infty}^0 e^q dq \\
&+ \tau_p \left(\frac{\partial u_i}{\partial t} + V_j(t) \frac{\partial u_i}{\partial x_j} \right) \int_{-\infty}^0 q e^q dq \\
&+ \tau_p^2 \left[\frac{1}{2} \frac{dV_j}{dt} \frac{\partial u_i}{\partial x_j} + \frac{1}{2} \left(\frac{\partial}{\partial t} + V_j(t) \frac{\partial}{\partial x_j} \right)^2 u_i \right] \int_{-\infty}^0 q^2 e^q dq + \mathcal{O}(\tau_p^3)
\end{aligned} \tag{3.30}$$

Carrying out the integrals yields the following expression:

$$\begin{aligned}
V_i(t; \mathbf{Y}(t) = \mathbf{x}) &= W_i^S + u_i(\mathbf{x}, t) \\
&\quad - \tau_p \left(\frac{\partial u_i}{\partial t} + V_j(t) \frac{\partial u_i}{\partial x_j} \right) \\
&\quad + \tau_p^2 \left[\frac{dV_j}{dt} \frac{\partial u_i}{\partial x_j} + \left(\frac{\partial}{\partial t} + V_j(t) \frac{\partial}{\partial x_j} \right)^2 u_i \right] + \mathcal{O}(\tau_p^3)
\end{aligned} \tag{3.31}$$

This result can be further extended to higher orders in τ_p . It represents an approximation of the particle velocity in terms of local fluid velocity and its gradients, as well as itself. The latter point implies that this is still not a closed form solution. The main assumptions we made so far are: (1) $\tau_p \ll t$; (2) the Taylor expansions for Y_i and u_i are valid. Since the field $u_i(\mathbf{x}, t)$ is smooth on the Kolmogorov scales, we anticipate that the above expression may even apply when $\tau_p \sim \tau_K$. But this last point is only true if the particle velocity is a single-valued function of its current location and time, which can be viewed as another condition for the validity of the above result. To proceed further, we strictly order the solution in terms of τ_p , assuming τ_p is small. We thus express the solution as

$$V_i(t; \mathbf{Y}(t) = \mathbf{x}) = V_i^{(0)}(t; \mathbf{Y}(t) = \mathbf{x}) + \tau_p V_i^{(1)}(t; \mathbf{Y}(t) = \mathbf{x}) + \tau_p^2 V_i^{(2)}(t; \mathbf{Y}(t) = \mathbf{x}) + \mathcal{O}(\tau_p^3) \tag{3.32}$$

Substituting this into equation 3.31, then order by order, we obtain

$$V_i^{(0)}(t; \mathbf{Y}(t) = \mathbf{x}) = W_i^S + u_i(\mathbf{x}, t) \tag{3.33}$$

and

$$V_i^{(1)}(t; \mathbf{Y}(t) = \mathbf{x}) = -\frac{\partial u_i}{\partial t} - V_j^{(0)} \frac{\partial u_i}{\partial x_j} = -\frac{\partial u_i}{\partial t} - [W_j^S + u_j(\mathbf{x}, t)] \frac{\partial u_i}{\partial x_j}. \tag{3.34}$$

Therefore, to the leading order $\mathcal{O}(\tau_p)$, we have

$$V_i(t; \mathbf{Y}(t) = \mathbf{x}) = W_i^S + u_i(\mathbf{x}, t) - \tau_p \left[\frac{\partial u_i}{\partial t} + (W_j^S + u_j(\mathbf{x}, t)) \frac{\partial u_i}{\partial x_j} \right] + \mathcal{O}(\tau_p^2) \tag{3.35}$$

or,

$$\boxed{V_i(t; \mathbf{Y}(t) = \mathbf{x}) = W_i^S + u_i(\mathbf{x}, t) - \tau_p \left[\frac{Du_i}{Dt} + W_j^S \frac{\partial u_i}{\partial x_j} \right] + \mathcal{O}(\tau_p^2)} \tag{3.36}$$

where

$$\frac{Du_i}{Dt} \equiv \frac{\partial u_i}{\partial t} + u_j \frac{\partial u_i}{\partial x_j}. \quad (3.37)$$

Equation 3.36 is the well-known result first obtained by Maxey (1987, Eq. (5.7)), and Eq. (1) in Balachandar and Eaton (2010). This is the equation we use for the asymptotic expansion method in our simulations.

3.3 Validation Of The Asymptotic Expansion For 2-D Cellular Flow

We use the asymptotic expansion technique for particle tracking first for a simpler 2-D cellular flow (as in Maxey, 87). We use the results for this simpler flow to validate our implementation. The cellular flow is described as:

$$u_1 = U_0 \sin\left(\frac{x_1}{2\pi}\right) \cos\left(\frac{x_2}{2\pi}\right) \quad (3.38)$$

$$u_2 = -U_0 \cos\left(\frac{x_1}{2\pi}\right) \sin\left(\frac{x_2}{2\pi}\right) \quad (3.39)$$

where u is the flow velocity, x is the position, and L is the length of a cell, subscripts 1, and 2 denote the x and y directions, respectively. 2π is the domain length in each direction. We consider the gravity to be in the x-direction. It should be noted that the fluid velocity in the particle location for this 2-D cellular flow is being directly calculated by using the position coordinates as opposed to the approximation by using the six point lagrangian interpolation method for the turbulent flow.

Figure 3.1 shows the particle trajectories for four particles, trajectories for two of the particles are calculated using the existing approach, and the other two of are calculated using the newly implemented asymptotic approach. Two sets of initial positions are used for each method, the reason for using 2 sets is to double check the results. The particle Stokes number in all the cases is 0.03, which is with in the valid range for the asymptotic expansion to work.

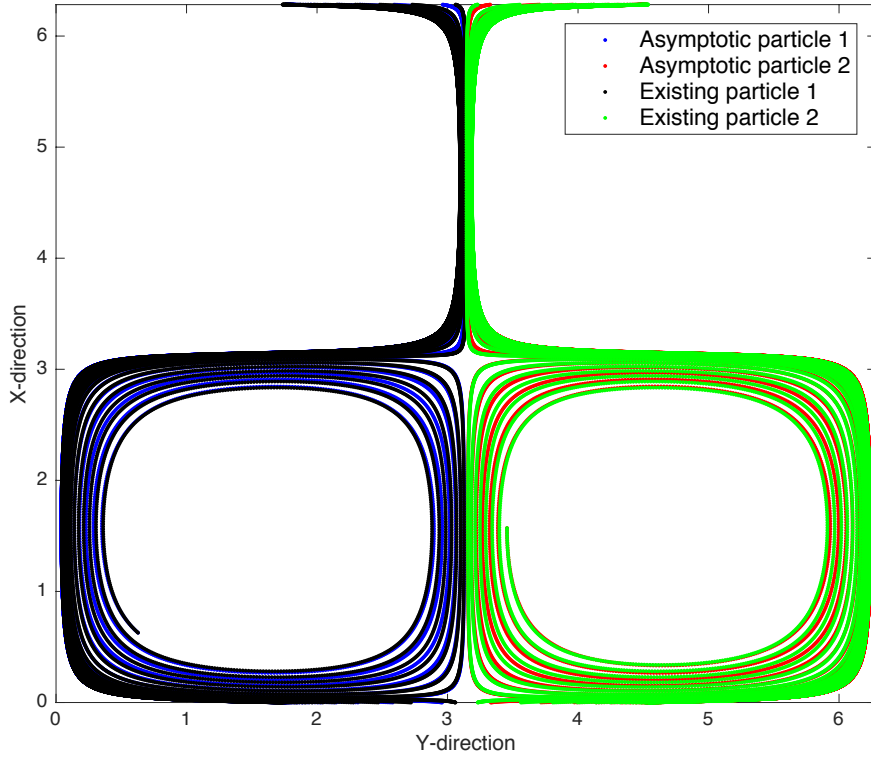


Figure 3.1: Particle trajectory comparison for asymptotic and existing approach in 2D cellular flow

In this case we are using 4-cells in the domain, 2 in each direction x and y . The particle trajectories in both methods are similar, which validates our implementation of the asymptotic approach. We plot the x -direction along the y -axis because in our code the gravity is in the x -direction. For further validation, we plot the relative error of $r = \sqrt{x^2 + y^2}$ for the two methods as a function of time in figure 3.2, where x and y are particle position at a given time. The error (y -axis) is normalized by the length of the domain (2π), and time (x -axis) is normalized by the particle response time τ_p . Although the error looks large on the plot, since this is a zoomed-in figure (axis values provides the details), the error can be concluded to be indeed very small. The reason

for the semi-sinusoidal shape of the plot is that, when the particles are turning they are not in the exact same position according to both methods, so the changes in the x and y values are high at that time, which makes the error value shoot up.

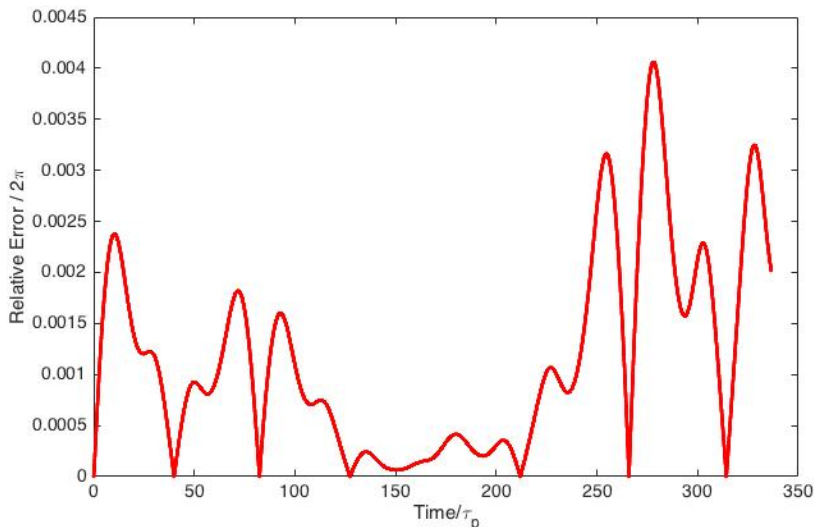


Figure 3.2: Relative error of position between the two methods as a function of time

3.4 Asymptotic Expansion In Turbulent Flow

With the validation of our implementation for the 2D cellular flow, we now use the same approach for a turbulent flow. Before we take a look at the results, we provide some information about the discretization time step size dt . As mentioned earlier in this chapter, that there are two time-scales, hence two different dt values, one is for the flow which is calculated based on the CFL condition for the flow simulation, and the other is for the particle which is typically taken as $dt_{particle} = 10\% \tau_p$, for the existing approach where τ_p is the particle inertial response time. So, the $dt_{simulation}$ is the minimum of dt_{flow} and $dt_{particle}$. By using the asymptotic expansion, we can relax $dt_{particle}$ dependence to some extent, and use larger values, however the dt_{flow} criteria remains same. In case of particles with low Stokes number, the $dt_{particle}$ is generally a

lot smaller than dt_{flow} . First we look at the comparison of the particle trajectories for a turbulent flow using the two approaches. Both simulations are for the same dissipation rate $\epsilon = 10cm^2/s^3$, both particles are of same Stokes number, $St = 0.01$, and they have the same initial position. We set $dt_{particle} = 10\% \tau_p$, for the existing approach, the τ_p chosen here is the smaller of the two particle sizes. For the asymptotic case, we plot trajectories by using larger dt sizes as well, typically we use $dt = 10\%, 20\%, 30\% \tau_p$, we also provide a comparison of a large time-step size ($dt = 10\% \tau_k$). It should be noted that we plot the trajectories up to the point in time when both of the particles are in the domain. As soon as the particle moves out of the domain, they are put back in the domain in a new position according to periodic boundary condition, so to avoid the complexity of the plot, we plot up to the point where in both particles are present in the domain from all three directions. Figure 3.3 shows the x vs y plot, and figure 3.4 shows the x vs z plot.

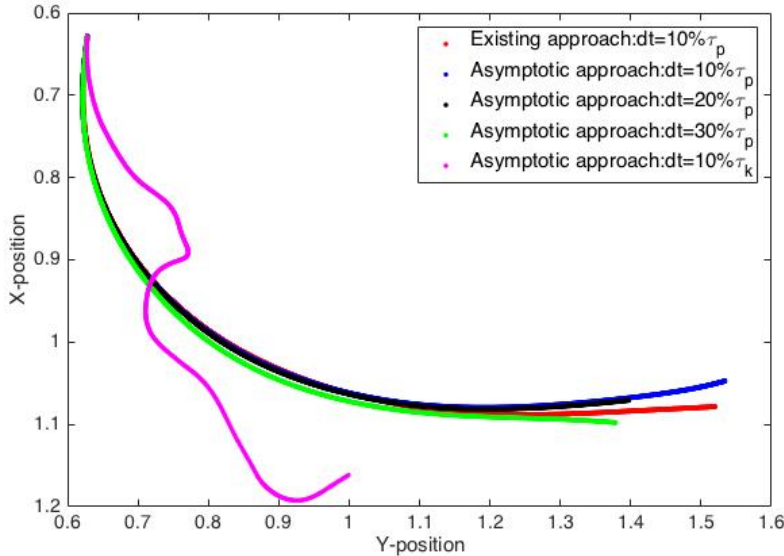


Figure 3.3: Particle trajectory comparison for asymptotic and existing approach in turbulent flow (x vs y)

The trajectories for both methods look similar qualitatively, we do not expect

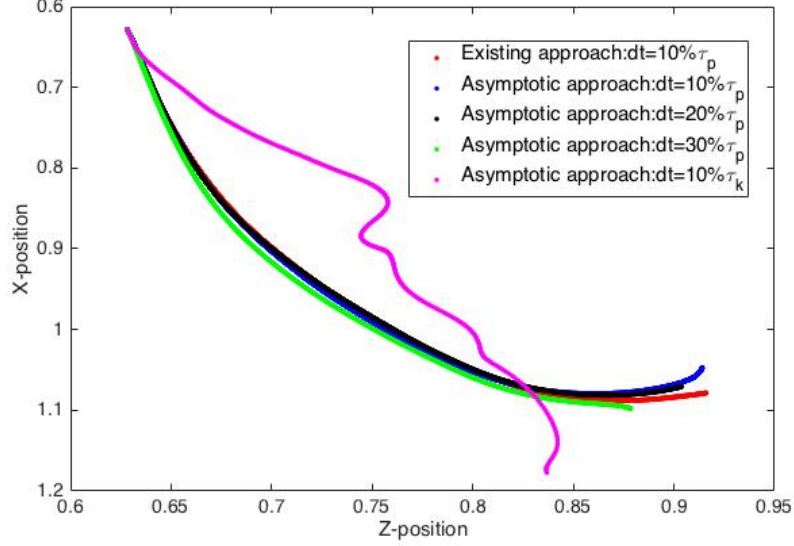


Figure 3.4: Particle trajectory comparison for asymptotic and existing approach in turbulent flow (x vs z)

an exact same trajectory in this case, as turbulent flow has a degree of randomness, and no two simulations would be exactly same. For the case of $dt = 10\%\tau_k$, we do expect a different trajectory, as the time-step size is very large in this compared to the others.

We also plot the relative error in the r-direction in x-y plane (calculated by $r = \sqrt{x^2 + z^2}$) in figure 3.5, and in x-z plane (calculated by $r = \sqrt{x^2 + z^2}$) in figure 3.6. The errors shown in the figures are relative to the direct integration method with a $dt = 10\%\tau_p$. The asymptotic methods were simulated at three different dt values, namely, $dt = 10\%$, 20% , $30\%\tau_p$, and $dt = 10\%\tau_k$. We expect larger error with increasing size of dt , and that is confirmed by the results.

Next we compare the collision statistics obtained for the two methods. For the collision statistics, we run the simulations at a dissipation rate of $\epsilon = 10\text{cm}^2/\text{s}^3$. The particle sizes are $10\mu\text{m}$ and $20\mu\text{m}$ in radius. The Stokes number are 0.01 and 0.04 respectively. We provide a comparison of the collision statistics for the existing

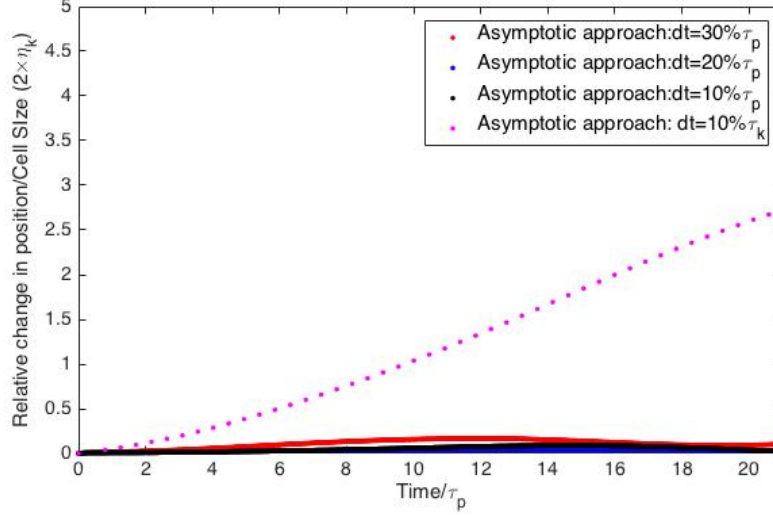


Figure 3.5: Relative error of r position (calculated by $r = \sqrt{x^2 + y^2}$) as a function of time for asymptotic method compared to the direct integration method

approach of our simulations (with $dt = 10\% \tau_p$) to the asymptotic approach (for $dt = 10\%, 20\%, 30\%$ of τ_p , and we provide a case of relatively large value of dt , where we set, $dt = 10\% \tau_k$, it should be noted that $\tau_k \sim 11.75 \times \tau_p$). We also provide the results for the same particle sizes, in the same flow dissipation rate as presented in Ayala et al 2008). Table 3.1 provides the results for the cross-size mean relative velocity of particles at contact in the radial direction along with the standard deviation.

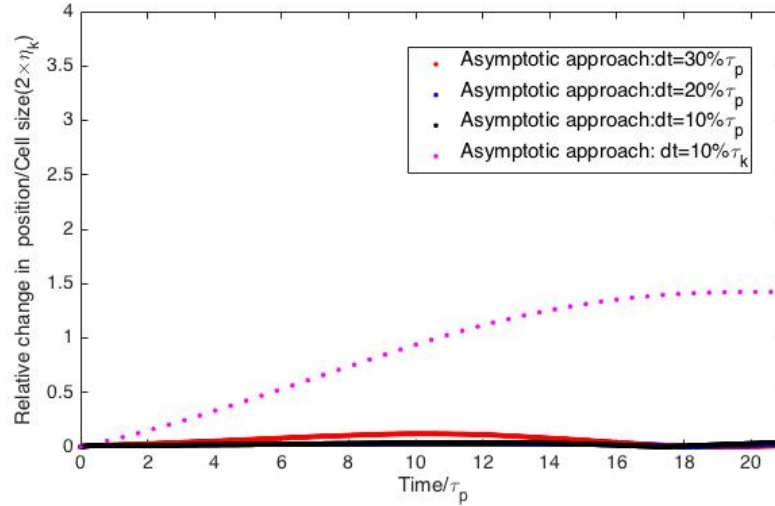


Figure 3.6: Relative error of r position (calculated by $r = \sqrt{x^2 + z^2}$) as a function of time for asymptotic method compared to the direct integration method

Table 3.1: Comparison of w_r for existing approach and asymptotic approach

Case	w_r	Standard Deviation
Ayala et al, 2008	1.8927	0.0843
Existing $dt = 10\% \tau_p$	1.9228	0.0016
Asymptotic $dt = 10\% \tau_p$	1.9239	0.0016
Asymptotic $dt = 20\% \tau_p$	1.9234	0.0023
Asymptotic $dt = 30\% \tau_p$	1.9131	0.0029
Asymptotic $dt = 10\% \tau_k$	1.9022	0.0181

The results for both approaches of our simulations is well with in the uncertainty limit of the published results in Ayala et al. In table 3.2 we provide a comparison for the cross-size radial distribution function (RDF), and its standard deviation for the same simulations.

Table 3.2: Comparison of RDF, $(g(r))$ for existing approach and asymptotic approach

Case	$g(r)$	Standard Deviation
Ayala et al, 2008	0.945	0.076
Existing $dt = 10\% \tau_p$	1.0034	0.0015
Asymptotic $dt = 10\% \tau_p$	0.9996	0.0015
Asymptotic $dt = 20\% \tau_p$	0.9980	0.0021
Asymptotic $dt = 30\% \tau_p$	1.0016	0.0026
Asymptotic $dt = 10\% \tau_k$	1.0092	0.0065

The results show very little difference with the published results in Ayala et al, 2008. There is a little difference between our existing approach and the asymptotic approach, however, that difference is very small.

Finally, we present the results for the collision-kernel. Table 3.3 shows the comparison for the cross-size collision kernel and its standard deviation for the same simulations.

Table 3.3: Comparison of collision kernel, (Γ) for existing approach and asymptotic approach

Case	Γ	Standard Deviation
Ayala et al, 2008	1.151E-04	4.01E-06
Existing $dt = 10\%\tau_p$	1.0911E-04	2.61E-07
Asymptotic $dt = 10\%\tau_p$	1.0875E-04	2.61E-007
Asymptotic $dt = 20\%\tau_p$	1.0855E-04	3.69E-07
Asymptotic $dt = 30\%\tau_p$	1.0835E-04	4.51E-07
Asymptotic $dt = 10\%\tau_k$	1.0856E-04	2.83E-06

There is a slight difference in the mean collision kernel from our results to that of Ayala et al. However, the percentage difference of the mean from our case is less than 5% to that of Ayala et al's results. It should be noted that the standard deviation of Ayala et al is higher, which when brought into consideration will bring down the percentage difference to an even lower value. Thus, we can conclude that our results are almost similar to that of Ayala et al.

3.4.1 Run time comparison

Table 3.4 shows a comparison of the run time of the existing approach with asymptotic approach for the different dt values for larger particle ($30\mu m$ and $440\mu m$ radius, in a flow of same dissipation rate $\epsilon = 10cm^2/s^3$). The total physical time for simulation is same for all the cases, so the number of time-steps varies.

Table 3.4: Comparison of run time for existing approach and asymptotic approach

Case	Run Time (in minutes)
Existing $dt = 10\%\tau_p$	972.67
Asymptotic $dt = 10\%\tau_p$	1278.43
Asymptotic $dt = 20\%\tau_p$	637.38
Asymptotic $dt = 30\%\tau_p$	429.01
Asymptotic $dt = 10\%\tau_k$	17.83

The results show that our implementation of asymptotic expansion is correct, and this could be used as an alternative to the existing approach for particles with low Stokes numbers. The run time comparison shows that with relaxing dt , we can speed up the code considerably, although it takes more time for the asymptotic expansion for the same number of time-steps as in the existing method due to some extra interpolations of the fluid velocity derivatives at the particle position, the relaxation of the dt enables us to gain more time eventually, which is the main advantage of the asymptotic expansion approach. Although we can relax the $dt_{particle}$ (here we have used up to $dt = 10\%$ of τ_k , it needs to be seen up to what percentage of τ_p will the results be still correct. This could be a direction for future work.

Chapter 4

SUMMARY AND CONCLUSION

This thesis focuses on collision statistics of cloud droplets in strato-cumulus clouds. We perform direct numerical simulations of the collision process of droplets in clouds. Typically we match the average dissipation rate, ϵ and the liquid water content, LWC to the clouds. So far very little work has been done specific to strato-cumulus clouds where the dissipation rate is relatively low. We provide results for collision statistics at low dissipation rates (as low as $\sim 3\text{cm}^2/\text{s}^3$) which are relevant to strato-cumulus clouds. Due to the expensive nature of the simulations, hence lack of DNS data, a linear interpolation model has been used to generate the collision statistics at a given low dissipation rate. The results for the low dissipation rates were interpolated linearly between dissipation rates of 0 and $100\text{cm}^2/\text{s}^3$, where the zero case corresponds to the gravity only case.

In our work, we first re-visit the gravity only case, and provide a rigorous formulation of the standard deviation of the collision kernel. We provide a validation of the collision detection scheme used in our simulations. The motivation to revisit the gravity only case was due to the fact that in case of weak turbulence, we expect the particle motion to be mostly driven by gravity. Hence the initial particle position configuration could affect the collision statistics. For low dissipation rates, we ran simulations at several dissipation rates in the range of 1-100 cm^2/s^3 , which is relevant to strato-cumulus clouds. We compare our results of the collision efficiency enhancement factor with the linear interpolation model. We find a non-linear dependence of the collision statistics on the dissipation rate, and we expect this to be due to the combination of the coupling of turbulence and hydrodynamic interactions.

In order to determine the exact reason for the non-linearity, we need to run more simulations, at low dissipation rates. However, as the low dissipation rate simulations are very expensive computationally, we implement the asymptotic expansion approach for particle tracking. In strato-cumulus clouds the particle Stokes number is relatively small, which makes the use of asymptotic expansion valid. We provide an alternative derivation of the asymptotic expansion implementation as used by Maxey, 87. We validate our implementation by first using the approach for a simpler flow: 2D cellular flow, and present the results for the particle trajectories for both methods of particle tracking. Next we compare particle trajectories for a turbulent flow using both methods. Then we compare the simulated collision statistics between the two methods, as well as against using published results (Ayala et al, 2008). The results show that the asymptotic expansion indeed produces reasonable results for the collision statistics. Finally we compare the CPU times of the two methods, and show the speed up using the asymptotic expansion as we can relax the dt size.

This work can be taken forward further, first by determining the percentage value of dt with respect to τ_p up to which the asymptotic expansion would still produce valid results. This would depend up on the particle Stokes number and the Reynolds number simulated for. So far we ran simulations for $dt = 10\% \tau_k$, for $Re_\lambda = 72.4$. It would also be interesting to determine the accuracy of the asymptotic expansion in case of higher Reynolds number, which would require better resolutions for the domain. The collision statistics using the existing approach could also be generated for higher Reynolds number, and a comparison of the two methods for collision statistics and the CPU time comparison would be something important. The asymptotic expansion method if found to be accurate for higher Reynolds number would be a step forward in the analysis of cloud physics relevant to strato-cumulus clouds, as the bottleneck due to the expensive nature of the simulations would be reduced to a considerable extent. Finally, the determination of the reason of the non-linearity in the collision efficiency enhancement factor results could be performed, and this could be an important contribution in the field of cloud physics.

REFERENCES

- Lau K.M and H.T. Wu “Warm rain processes over tropical oceans and climate implications.” *Geophys. Res. Lett.* 30, 2290-2294, 2003.
- Shivshankar Sundaram and Lance Collins “Collision statistics in an isotropic particle-laden turbulent suspension. Part 1. Direct numerical simulations” *JFM*, 1997.
- Lian-Ping Wang, Anthony S. Wexler, Y. Zhou “On the collision rate of small particles in isotropic turbulence. I. Zero-inertia case” *Phys. of Fluids*, 1998.
- Lian-Ping Wang, Anthony S. Wexler, Y. Zhou “Statistical Mechanical Descriptions of Turbulent Coagulation of Inertial Particles.” *JFM*, 2000.
- Pruppacher H.R. and Klett J.D, “Microphysics of clouds and precipitation” *Kluwer Academic Publishers*, 1997.
- Grabowski and Wang, “Growth of cloud droplets in a turbulent environment.” *Annu. Rev. Fluid Mech.*, 2013.
- L.-P. Wang, O. Ayala, S.E. Kasprzak, and W.W. Grabowski, “Theoretical formulation of collision rate and collision efficiency of hydrodynamically-interacting cloud droplets in turbulent atmosphere” *J. Atmos. Sci.*, 2005.
- L.-P. Wang, O. Ayala, B. Rosa, W.W. Grabowski, “Turbulent collision efficiency of heavy particles relevant to cloud droplets.” *New J. Physics*, 2008.
- Szumowski, Rauber, Ochs, Miller, “The microphysical structure and evolution of Hawaiian rainband clouds.1: Radar observations of rainbands containing high reflectivity cores” *J. Atmos. Sci.*, 1997.
- Rauber, Knight, Ochs, Stevens, “RICO: Rain in cumulus over ocean experiment”, 2003.
- Knight, Vivekanandan, Lasher-Trapp “First radar echoes and the early Z_{DR} history of florida cumulus. *J. Atmos. Sci.*, 2002.

- O. Ayala, B. Rosa, L.-P. Wang, W.W. Grabowski, "Effects of Turbulence on the Geometric Collision Rate of Sedimenting Droplets: Part 1. Results from direct numerical simulation" *New J. Physics*, 2008.
- O. Ayala, B. Rosa, L.-P. Wang, "Effects of Turbulence on the Geometric Collision Rate of Sedimenting Droplets: Part 2. Theory and Parameterization." *New J. Physics*, 2008.
- L.-P. Wang, O. Ayala, and W.W. Grabowski, "Improved formulations of the superposition method", *J. of the Atmospheric Sciences*, 2005
- L.-P. Wang, C.N. Franklin, O. Ayala, W.W. Grabowski, " On probability distributions of angle-of-approach and relative velocity for colliding droplets in a turbulent flow.", *J. of the Atmospheric Sciences*, 2006.
- L.-P. Wang, O. Ayala, and W.W. Grabowski, "Effects of aerodynamic interactions on the motion of heavy particles in a bidisperse suspension.", *Journal of Turbulence*, 2007.
- L.-P. Wang, B. Rosa, H. Gao, G.W. He, G.D. Jin, "Turbulent collision of inertial particles: point-particle based, hybrid simulations and beyond" *Int. J. Multiphase Flow*, 2009.
- L.-P. Wang and W.W. Grabowski, "The role of air turbulence in warm rain initiation." *Atmospheric Science Letters*, 2009.
- Maxey M.R, "The motion of small spherical particles in a cellular flow field" *Phys. of Fluids*, 1987.
- Maxey M.R, "The gravitational settling of aerosol particles in homogeneous turbulence and random flow fields" *JFM*, 1987.
- Khain A.P, M.B. Pinsky, "Turbulence effects on the collision kernel II. Increase of the swept volume of colliding drops", *Quarterly journal of the Royal Meteorological Society*, 1997.
- Koizol A.S, Leighton H. G, "The effects of turbulence on collision rate of small cloud droplets" *J. Atmos. Sci*, 1996.
- Rauber, R.M & co-authors, "Rain in shallow cumulus over the ocean: The RICO campaign." *Bull. Amer. Meteor. Soc*, 2007.

- Almeida, F.C. de, “The collisional problem of cloud droplets moving in turbulent environment: Part I: Method of solution”, *Journal of Atmos. Sci.*, 1976.
- Almeida, F.C. de, “The collisional problem of cloud droplets moving in turbulent environment: Part II: Turbulent collision efficiencies”, *Journal of Atmos. Sci.*, 1979.
- Pinsky M.B., A.P. Khain, and M. Shapiro, “Collision of small drops in a turbulent flow, Part I: Collision Efficiency, Problem formulation and preliminary results”, *Journal of Atmos. Sci.*, 1999.
- Pinsky M.B., A.P. Khain, and M. Shapiro, “Stochastic effect of cloud droplet hydrodynamic interaction in a turbulent flow”, *Atmos. Res.*, 2000.
- L.-P. Wang, M. R. Maxey, “Settling velocity and concentration distribution of heavy particles in homogenous isotropic turbulence”, *JFM*, 1993.